# Rational Design of an Optimal Al-substituted Layered Oxide Cathode for Na-ion Batteries

Hari Narayanan Vasavan <sup>a</sup>, Manish Badole <sup>a</sup>, Samriddhi Saxena <sup>a</sup>, Velaga Srihari <sup>b</sup>, Asish Kumar Das <sup>a</sup>, Pratiksha Gami <sup>a</sup>, Neha Dagar <sup>a</sup>, Sonia Deswal <sup>c</sup>, Pradeep Kumar <sup>c</sup>, Himanshu Kumar Poswal <sup>b</sup>, and Sunil Kumar <sup>a,d,\*</sup>

<sup>a</sup> Department of Metallurgical Engineering and Materials Science, Indian Institute of Technology Indore, Simrol, 453552, India.

<sup>b</sup> High Pressure & Synchrotron Radiation Physics Division, Bhabha Atomic Research Centre, 400085 Mumbai, India

<sup>c</sup> School of Physical Sciences, Indian Institute of Technology Mandi, Himachal Pradesh, 175005, India

<sup>d</sup> Center for Electric Vehicle and Intelligent Transport Systems, Indian Institute of Technology Indore, Simrol, 453552, India.

\* Corresponding Author: sunil@iiti.ac.in

## **Abstract**

Layered oxide cathodes, a promising avenue for Na-ion batteries, hold the highest potential for commercialization. Herein, we delve into the structural and electrochemical properties of Alsubstituted layered oxides in our quest to pinpoint the optimal cathode composition in the Na<sub>3/4</sub>(Mn-Al-Ni)O<sub>2</sub> pseudo-ternary system. The cathode materials investigated were synthesized in three distinct phase configurations, which include two monophasic configurations with P3 and P2-type structures and a third biphasic cathode with equal proportions of P3 and P2 phases. The fractions of the P3 and P2 type phases in the cathode materials were manipulated by adjusting the calcination temperature. The varying concentration of Mn<sup>3+</sup> and Mn<sup>4+</sup>, confirmed by X-ray photoelectron spectroscopy, was found to impact the cyclic stability of these materials significantly. During electrochemical testing, the P3 cathodes showed impressive rate performance and exhibited an excellent specific capacity of 195 mAh g<sup>-1</sup> at 0.1C. Regarding cyclic performance, the biphasic cathodes outperformed consistently their monophasic counterparts, with P3/P2-Na<sub>0.75</sub>Mn<sub>0.50</sub>Ni<sub>0.25</sub>Al<sub>0.25</sub>O<sub>2</sub> exhibiting 82% capacity retention after 300 cycles. Analysis of operando Synchrotron XRD data revealed an absence of P3 to O3 type phase transition in the cathodes even at low voltages where large structural variations to the unit cell structure were observed. The absence of P3 to O3 transformations and the superior electrochemical performance of Na<sub>0.75</sub>Mn<sub>0.50</sub>Ni<sub>0.25</sub>Al<sub>0.25</sub>O<sub>2</sub> underlines the importance of Al substitution and P3/P2 biphasic structure in enhancing the electrochemical performance of layered oxides.

**KEYWORDS**: Electrochemistry; Layered compounds; Biphasic; *Operando* Synchrotron XRD;

## 1.0. Introduction

Na-ion batteries (NIBs) are often considered ideal candidates to complement or replace Li-ion batteries [1, 2]. With the demand for energy storage systems rising by the day, NIBs can offer a cheaper alternative to the current lithium-based energy storage systems, especially for stationary storage applications [3-8]. Currently, the primary bottleneck towards the commercialization of NIBs arises from the relatively lower energy density of their cathode materials [6, 9-11]. Cathode materials in Na-ion batteries are divided into three material classes: layered oxides, NASICON, and Prussian blue analogs [12, 13]. Even though NASICON and Prussian blue analog-type cathodes have seen intense research activity over the past decade, layered oxide cathodes are still considered the popular choice for commercialization in Na-ion batteries [3, 7, 13-15]. This is mainly due to their higher energy density, ease of synthesis, and compositional diversity. Layered oxides (LOs), having a general formula of Na<sub>x</sub>TMO<sub>2</sub>;  $0 < x \le 1$ ; TM- transition metal cations, are synthesized in different structures. P2, P3, O3 [16-19]. The P-type phases normally have a lower Na concentration (typically less than 0.75). Na-ions occupy prismatic sites in these phases, resulting in higher Na-ion diffusion rates and lower activation energies [20-24]. In contrast, Na-ions in O3 phases occupy octahedral sites and can accommodate higher Na concentrations (hence exhibit better specific capacities) but suffer from poor Na<sup>+</sup> transport properties [18, 25-27].

Biphasic cathodes containing both P-type and O-type phases are proposed as a possible solution to enhance the electrochemical performance of layered oxides. The most common types of biphasic cathodes often found in the literature are those based on P2 and O3-type structures [28-33]. In addition to the improved specific capacity and Na<sup>+</sup> diffusion, the synergistic effect arising from the coexistence of 2 phases also reportedly improves the structural stability of these cathodes, which boosts their cyclic performance. Although not extensively studied, biphasic cathodes involving P2/P3 type phase materials also show similar improvements in

electrochemical performance due to the synergistic effects [28, 34-37]. In addition to a biphasic structure, the incorporation of electrochemically inactive ions, such as Al<sup>3+</sup>, Zn<sup>2+</sup>, Mg<sup>2+</sup>, Ti<sup>4+</sup>, etc., into the transition metal layers is also a common technique explored for enhancing the electrochemical performance of layered oxide cathodes [23, 37-42]. Such inactive ions act as pillars during the interaction and deintercalation of Na-ions and have been reported to improve the cyclic stability of LO compounds. Although scarcely explored in NIBs, substituting transition metal ions with Al<sup>3+</sup> has been widely reported to enhance the electrochemical performance of LO-based cathodes in LIBs [43-46].

The current study explores trends in the structural and electrochemical performance of various compositions in the Na<sub>3/4</sub>(Mn-Al-Ni)O<sub>2</sub> pseudo-ternary system (Fig. 1) to identify optimal cathodes. All the compositions were synthesized in 3 different phase configurations: monophasic P3, biphasic P3/P2, and monophasic P2. Na<sub>0.75</sub>Mn<sub>0.75</sub>Ni<sub>0.25</sub>O<sub>2</sub> and Na<sub>0.75</sub>Mn<sub>0.75</sub>Al<sub>0.25</sub>O<sub>2</sub> (marked as NMA1 and NMA2 in Fig. 1) were the parent materials chosen for the study. The structural and electrochemical properties of Na<sub>0.75</sub>Mn<sub>0.75</sub>Ni<sub>0.25</sub>O<sub>2</sub> and Na<sub>0.75</sub>Mn<sub>0.75</sub>Al<sub>0.25</sub>O<sub>2</sub> can be found elsewhere [35, 47]. The concentration of the Jahn-Teller active Mn<sup>3+</sup> and commonly preferred Mn<sup>4+</sup> ions vary across all the compositions, which may significantly affect the electrochemical properties of the cathode materials. The adoption of a P3/P2 biphasic structure, along with the incorporation of A1<sup>3+</sup>, is expected to mitigate the effects of the structural distortions caused by the presence of Mn<sup>3+</sup> in the layered oxide structure. Additionally, recent studies have indicated that the substitution of Al<sup>3+</sup> in P2 phases decreases the TM-O<sub>6</sub> octahedral volume structures while increasing the volume of Na-O<sub>6</sub> prisms, leading to improved rate performance[48]. Hence, the systematic analysis of various compositions in the Na<sub>3/4</sub>(Mn-Al-Ni)O<sub>2</sub> pseudo-ternary system would help identify an optimal Al concentration and unravel performance trends across the pseudo-ternary diagram as a consequence of different element concentrations.

## 2.0. Materials and Methods

The materials were obtained through a conventional sol-gel synthesis method, using aluminum nitrate nonahydrate, manganese (II) acetate tetrahydrate, nickel acetate tetrahydrate, and sodium carbonate as precursors. Appropriate amounts of these compounds were dissolved in deionized water and stirred, followed by adding ethylene glycol and citric acid. The resulting solution was heated to produce a gel, which was dried and calcinated at varying temperatures (650 – 900 °C) to obtain the final product. The Al-substituted compounds synthesized for the study, Na<sub>0.75</sub>Mn<sub>0.5</sub>Ni<sub>0.25</sub>Al<sub>0.25</sub>O<sub>2</sub>, Na<sub>0.75</sub>Mn<sub>0.625</sub>Ni<sub>0.125</sub>Al<sub>0.25</sub>O<sub>2</sub>, Na<sub>0.75</sub>Mn<sub>0.625</sub>Ni<sub>0.125</sub>Al<sub>0.125</sub>O<sub>2</sub>, and Na<sub>0.75</sub>Mn<sub>0.75</sub>Ni<sub>0.125</sub>Al<sub>0.125</sub>O<sub>2</sub> are a part of the Na<sub>3/4</sub>(Mn-Al-Ni)O<sub>2</sub> pseudo ternary diagram and will henceforth be referred to as NMA3, NMA4, NMA5 and NMA6, respectively.

Inductively coupled plasma atomic emission spectrometry (ICP-AES) (SPECTRO Analytical Instruments GmbH, Germany, Model: ARCOS, Simultaneous ICP Spectrometer) was used to determine the specific chemical compositions of the cathode materials. The X-ray diffraction (XRD) data were recorded using a Malvern Pan Analytical Empyrean diffractometer (Cu-Kα radiation source) at room temperature. The XRD data were analyzed using Rietveld refinement with the help of the *TOPAS Academic* (version 6) software package [49]. The microstructural studies were conducted using a JEOL field emission scanning electron microscope (model JEOL-7610). The Mn 2p and Ni 2p X-ray photoelectron spectra (XPS) were collected from a Thermofisher Scientific - Naxsa base with an Al Kα X-ray source (1486.6 eV). *Operando* Synchrotron XRD patterns were obtained at the extreme conditions angle dispersive/energy dispersive synchrotron X-ray diffraction beamline (BL11) at Indus-2 (RRCAT) with a beam wavelength of 0.6645 Å and 0.74 Å for NMA3-P3P2 and NMA5-P3P2, respectively.

The electrochemical experiments were carried out using a Neware battery tester (CT-4008T) on half cells with 1M NaClO<sub>4</sub> in ethylene carbonate-propylene carbonate (vol. ratio of 1:1) acting as the electrolyte and a Whatman GF/D filter paper as the separator. The cathode was prepared by casting a slurry containing 75 wt% active material, 10 wt.% Ketjen black, and 15 wt.% PVDF (in a wt. ratio of 75:10:15) onto an Al current collector. The mass loading for the samples was  $\sim$  4-5 mg cm<sup>-2</sup>, and C-rates were calculated taking the nominal capacity of 150 mAh g<sup>-1</sup>. An NF Corp LCR meter (model: ZM 2376) was used to obtain the impedance data in the 1 Hz – 1 MHz frequency range at room temperature.

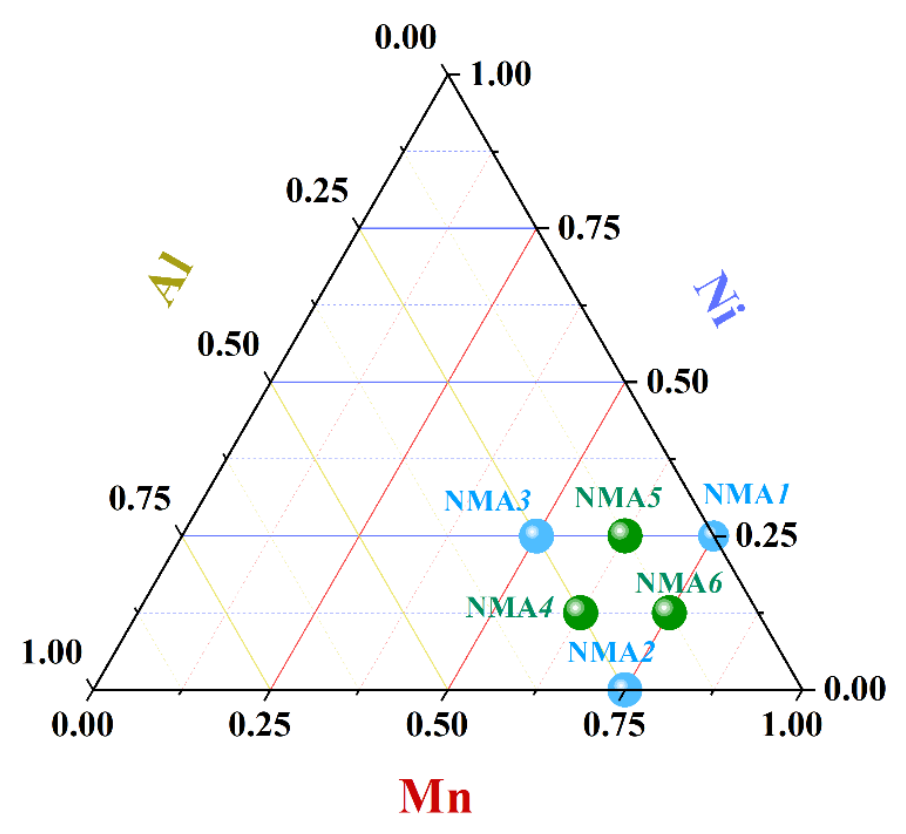


Fig. 1. The positions of compositions under investigation in this study in the pseudo-ternary  $Na_{3/4}(Mn-Al-Ni)O_2$  system.

## 3.0. Results and Discussion

# 3.1. Structural Characteristics

The NMAx series of cathode materials were synthesized through the sol-gel route. Each cathode material is synthesized in 3 different phase configurations, namely P3, P2, and P3/P2 mixed phase with equal proportions. This was achieved by calcinating the samples at optimum temperatures (by a trial-and-error process). Table S1 summarizes the ICP-AES data of P2 type NMAx series of cathode materials. The results from ICP concurred with the expected compositions of each of the cathodes.

Fig. 2 displays the room temperature XRD patterns of NMAx cathodes calcinated at different temperatures. The figure shows peaks consistent with a P3-type structure at 650 °C, transforming into a P2-type structure at higher calcination temperatures. A similar phase evolution in Na<sub>0.75</sub>Mn<sub>0.75</sub>Ni<sub>0.25</sub>O<sub>2</sub> (NMA*I*) and Na<sub>0.75</sub>Mn<sub>0.75</sub>Ni<sub>0.25</sub>O<sub>2</sub> (NMA2) compounds was reported earlier [35, 47]. Additionally, 0.75 Na was identified as the critical concentration of sodium at which an O3-type phase can be avoided during synthesis. The detailed analysis of the crystal structure and quantification of phase concentrations in the monophasic and P3/P2 mixed-phase samples was performed using the Rietveld refinement of XRD data (Fig. 3 and Fig. S1, S2). The crystallographic information for each of the NMA3-NMA6 materials is given in Tables S1-S4. The refinement confirmed the biphasic nature of the NMAx-P3P2 series of cathodes with close to 50% P3 and P2 phases. It also established the presence of only monophasic P3 (*R*3*m* space group) and P2-type (*P*6<sub>3</sub>/*mmc* space group) phases at the lower (< 750 °C) and high calcination temperatures, respectively, in all compositions.

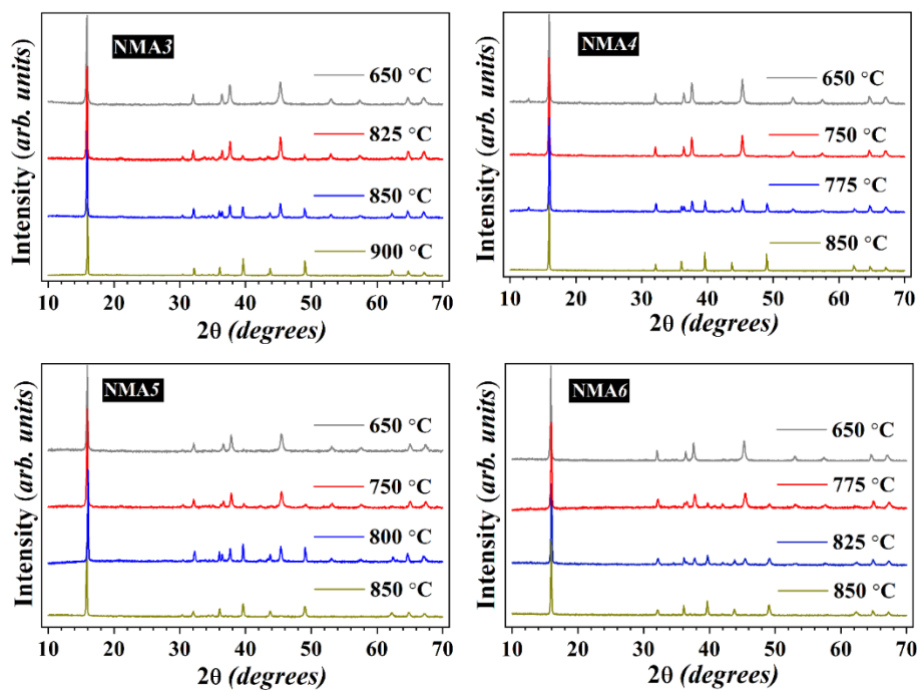


Fig. 2. Structural evolution of NMA3, NMA4, NMA5, and NMA6 cathode materials with calcination temperature.

The varying concentrations of Mn<sup>3+</sup> in the NMA*x* series have been identified by analyzing their Mn 2p Xray photoelectron spectra (Fig. 4). The Mn 2p XPS spectra of NMA*4* to NMA*6* are deconvoluted into 4 peaks at 641.8 & 653.2 eV and 643.2 & 654.7 eV belonging to Mn<sup>3+</sup> and Mn<sup>4+</sup>, respectively [50-52]. The increasing intensity of the deconvoluted Mn<sup>3+</sup> peaks from NMA*4* to NMA*5* and NMA*6* points to a rising concentration of Mn<sup>3+</sup> in these compounds. Unlike the other samples, the Mn 2p spectra of NMA*3* are fitted with only 2 peaks at 643.2 and 654.7 eV belonging to Mn<sup>4+</sup>, indicating the absence of Mn<sup>3+</sup>. The nominal concentration of Mn<sup>3+</sup> and Mn<sup>4+</sup> in the NMA series of cathodes is summarised in Table S6, and analysis of XPS data fitting indicates that the Mn<sup>3+</sup> and Mn<sup>4+</sup> fractions match closely with expected values within the acceptable error margins. Additionally, the Mn 2p spectra of P3-type samples in the NMA*x* series resemble their corresponding P2-type counterparts. This suggests a negligible Na loss during the calcination of P2-type samples, as a loss of Na during calcination would have increased the Mn<sup>4+</sup> concentration in these materials, leading to alterations in the peaks in the

Mn 2p spectrum. The Ni 2p XPS spectra of the NMAx samples displayed in Fig. S3 show similar peak energies, indicating the presence of only Ni<sup>2+</sup> in all samples [50-52].

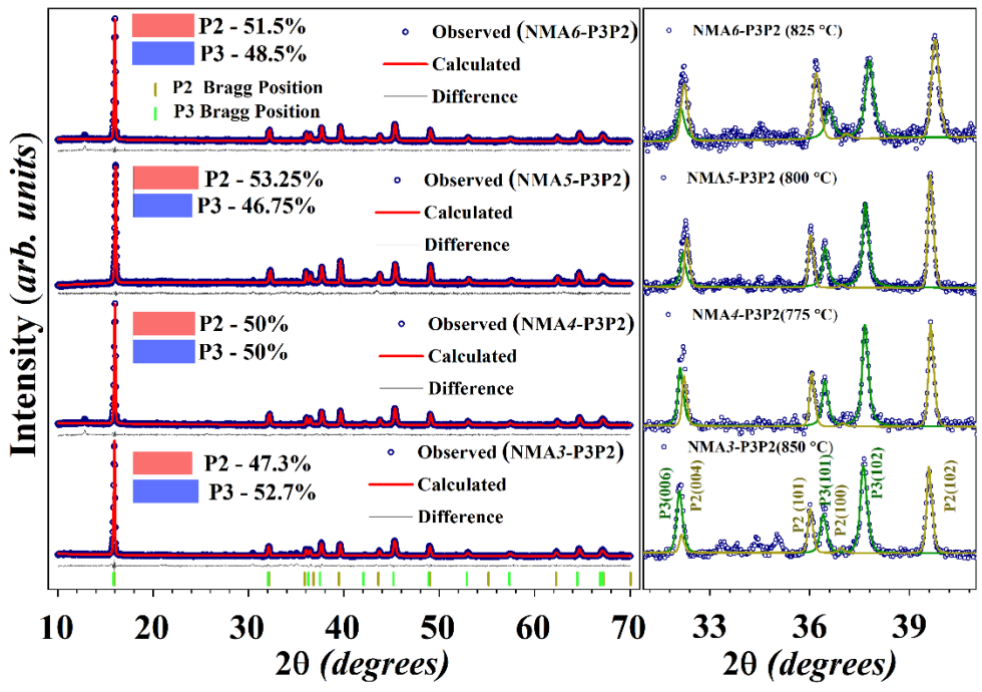


Fig. 3. Rietveld refinement of XRD data for NMA3-P3P2, NMA4-P3P2, NMA5-P3P2, and NMA6-P3P2 samples with their respective along with the deconvoluted P2 and P3 phases in the  $2\theta$  range of  $30\text{-}40^\circ$ .

The microstructural and morphological characteristics of the cathode materials were observed using FESEM, and the micrographs are displayed in Fig. 5 and Fig. S4. The SEM images of the P3 and P3/P2 mixed-phase samples show spheroidal and hexagonally shaped particles with a relatively lower degree of agglomeration. With increased calcination temperature, agglomeration increases, resulting in large particle clusters in the P2-type samples. Typically, materials with smaller particle sizes are preferred in cathode materials as these enhance the rate performance and cyclic stability of the electrode materials [53, 54]. Accordingly, it is expected that P3 and P3/P2 mixed-phase cathodes would exhibit better electrochemical performance than their P2 counterparts. The elemental maps of NMA5-P3P2 displayed in Fig. 4 show a homogeneous distribution of all its constituent elements.

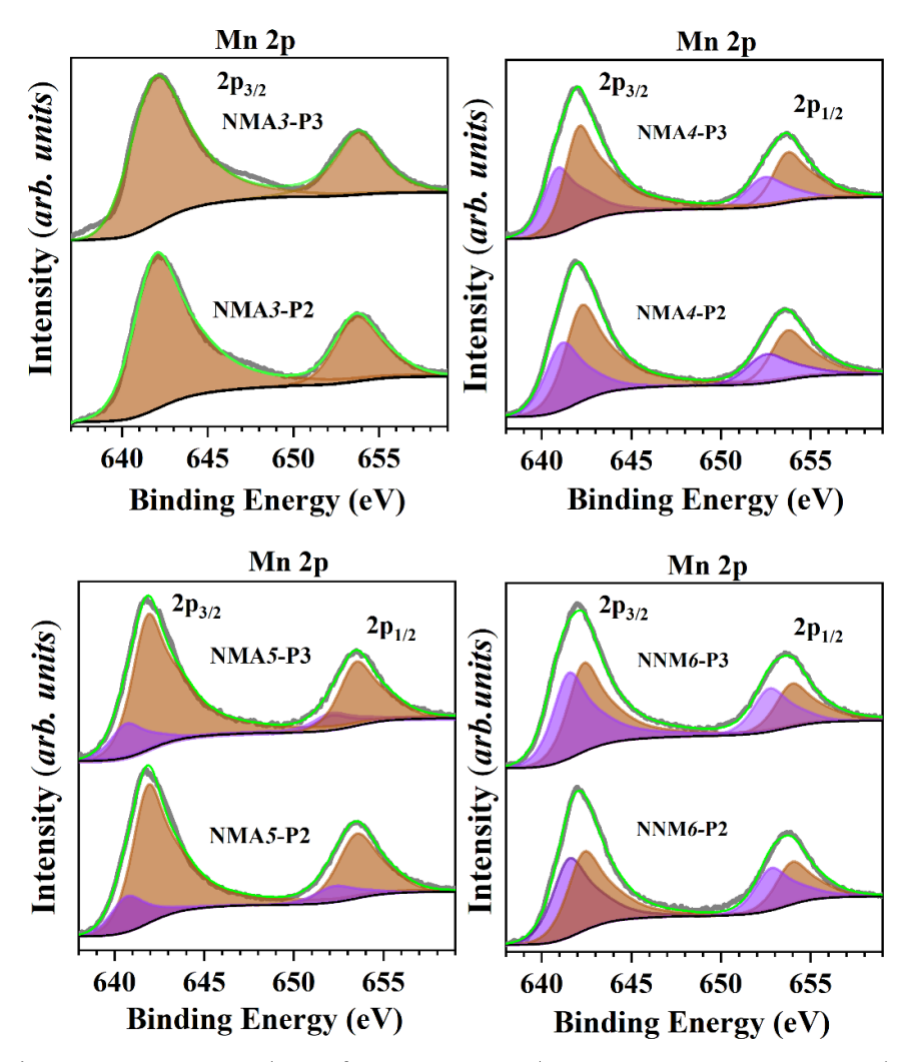


Fig. 4. Mn 2p XPS plots of NMAx-P3 and NMAx-P2 type compounds.

# 3.2. Electrochemical Characteristics

The galvanostatic charge-discharge (GCD) curves of NMAx samples cycled at different C rates between 1.5 V and 4.0 V are depicted in Fig. 6 and Fig. S5-S6. The cathodes were cycled in a half-cell configuration with Na metal as the counter electrode. The GCD curves depicting the first charge-discharge profiles of the NMAx series of cathodes are presented in Fig. S7. The initial columbic efficiency of all the cathodes is higher than 100% because of the increasing reduction of Mn<sup>4+</sup> ions when the concentration of Na<sup>+</sup> exceeds 0.75 in these samples during the discharge process.

Among different cathodes in the NMA*x* series, the NMA*3*-P3 and NMA*5*-P3 stand out in terms of their specific capacities. At a charge-discharge rate of 0.1C, both the cathodes show specific capacities close to 195 mAh g<sup>-1</sup> due to the higher Ni concentrations (Fig. 6(a1) and (b1)). This is validated by multiple peaks appearing in their respective CV and dQ/dV vs V plots above 3 V (Fig. S8 and S9) that correspond to Ni<sup>2+/4+</sup> redox couples [52, 55-57]. In contrast, the lower concentration of Ni<sup>2+</sup> in NMA*4* and NMA*6* cathodes limited their specific capacity to 170 mAh g<sup>-1</sup> at 0.1C. Moreover, unlike NMA3-P3 and NMA*5*-P3, more than 50% of the specific capacity in NMA*4*-P3 and NMA*6*-P3 is due to the activation of Mn<sup>3+/4+</sup> redox couples, which could lead to lower cyclic performance in the latter.

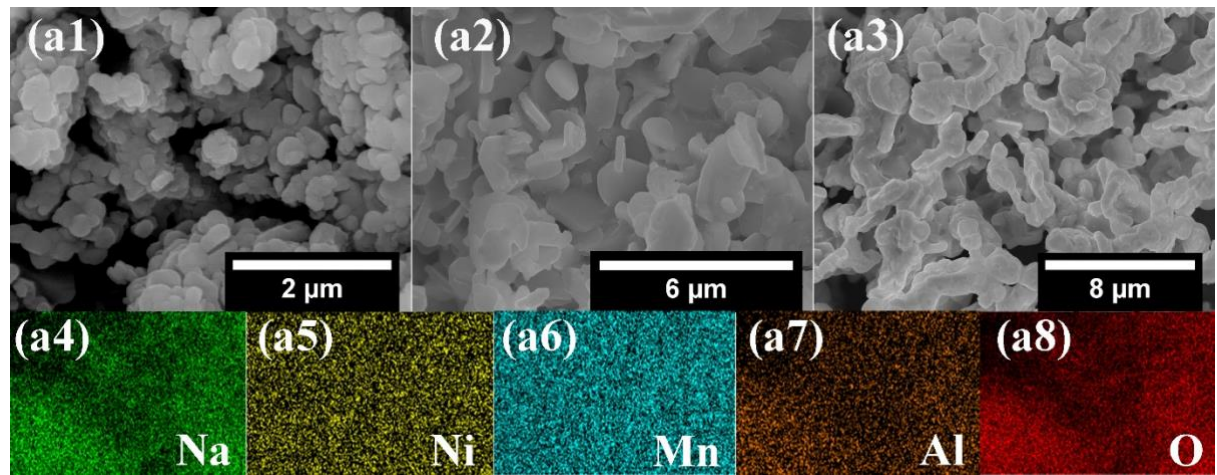


Fig. 5. SEM micrographs of (a1-a3) NMA5-P3, NMA5-P3P2, and NMA5-P2 with (a4-a8) depicting the elemental maps of the NMA5-P3P2 sample.

With an increase in the P2 phase concentration, the specific capacities of all the cathode materials show a decreasing trend. In NMA3-P3P2 and NMA5-P3P2, the specific capacities drop to  $\sim 175$  mAh g<sup>-1</sup>, further decreasing to  $\sim 150$  mAh g<sup>-1</sup> in NMA3-P2 and NMA5-P2. We had earlier reported such reductions in specific capacities with an increase in P2 phase concentration in both NMA1 and NMA2 compounds, which was attributed to the ability of the P3 phase to accommodate more Na ions by transforming to an O3 type phase, as in the case of NMA1-P3 [35, 47].

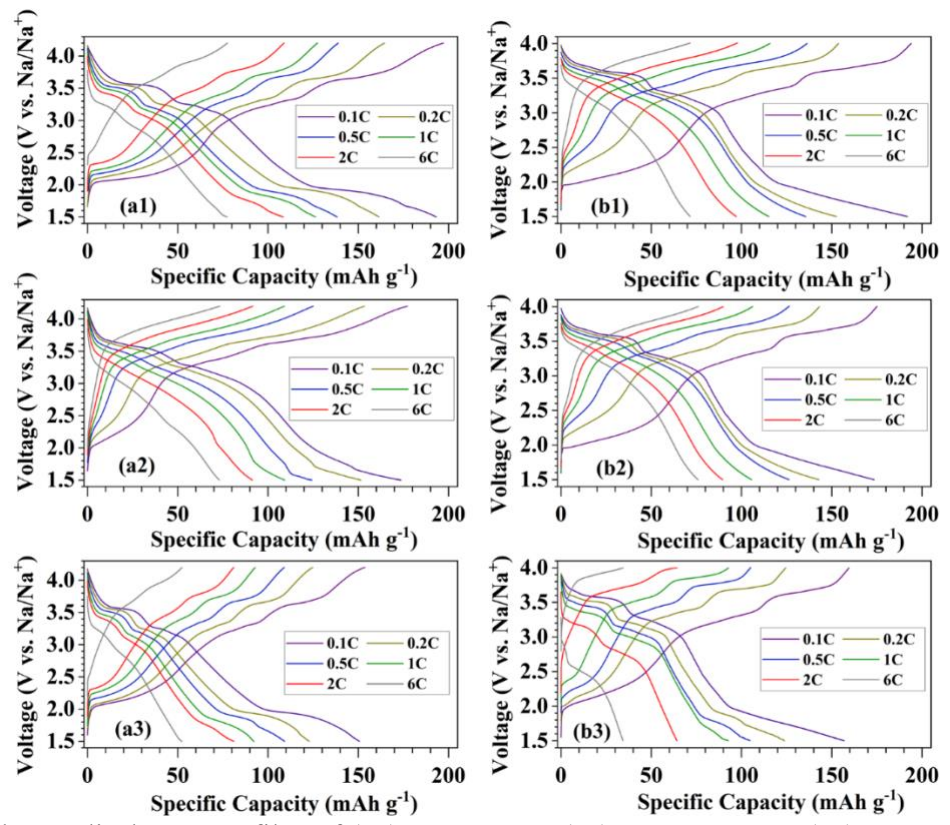


Fig. 6. Charge discharge profiles of (a1) NMA3-P3, (a2) NMA3-P3P2, (a3) NMA3-P2 (b1) NMA5-P3, (b2) NMA5-P3P2, (b3) NMA5-P2 series of cathodes at different C rates.

Regarding other electrochemical performance parameters, such as rate performance, unlike NMA*I* and NMA*2*, the monophasic P3 type cathodes of the NMA*x* compounds showed marginally better rate performance than their corresponding P3/P2 mixed-phase counterparts (Fig. 7(a-b) and Fig. S10(a-b)). At a discharge rate of 1C, NMA*3*-P3 and NMA*5*-P3 exhibited a specific capacity of 126 mAh g<sup>-1</sup> and 115 mAh g<sup>-1</sup>, respectively. At a higher discharge rate of 6 C, NMA*3*-P3 and NMA*5*-P3 and their P3/P2 mix phase compounds could sustain a specific capacity of ~ 77 mAh g<sup>-1</sup>. Meanwhile, in the NMA*4* and NMA*6* type cathodes, their P3 and P3/P2 mix phased compounds showed much lower capacities, close to 95 mAh g-1 at 0.1 C and 60 mAh g<sup>-1</sup> at 6C. Another notable feature of the rate performance curves is the consistently poor capacities exhibited by the P2-type cathodes. In all compositions, P2-type phases showed higher drops in specific capacities with an increase in discharge current, which could be attributed to large particle agglomerations in the P2 materials.

Even though the P3-type cathodes showed a relatively high specific capacity and rate performance, their cyclic stability was surprisingly underwhelming. Fig. 7(c-d) and Fig. S10(cd) depict the cyclic performance of the NMAx series of cathode materials at 1C between 1.5 V and 4.0 V. The biphasic P3/P2 type cathodes consistently retain higher capacity than their P3 and P2 counterparts in all the compounds. For instance, in NMA3 and NMA5 cathodes, NMA3-P3/P2 and NMA5-P3/P2 showed ~ 70% capacity retention after 300 cycles, while their P3 and P2 type cathodes retained less than 60% of their initial specific capacities, at 1C. Cyclic performance drops even in the case of NMA4-P3P2 and NMA6-P3P2, where capacity retention is only about 60% of the initial capacity after 300 cycles. This could be due to the increased activity of Mn3+/4+ redox couples in NMA4 and NMA6, which is known to cause large variations in unit cell volume during cycling. The interlocking between the P3 and P2 phases may aid in minimizing this large variation in unit cell volume at low voltages in the mixedphase samples, allowing these to achieve higher cyclic stabilities. Table S7 compares the electrochemical properties of various layered oxide cathode materials reported in literature. Even with the activation of Mn<sup>3+/4+</sup> redox couples, biphasic NMA3 and NMA5 cathodes showed superior cyclic performance compared to many of the reported layered oxide compounds.

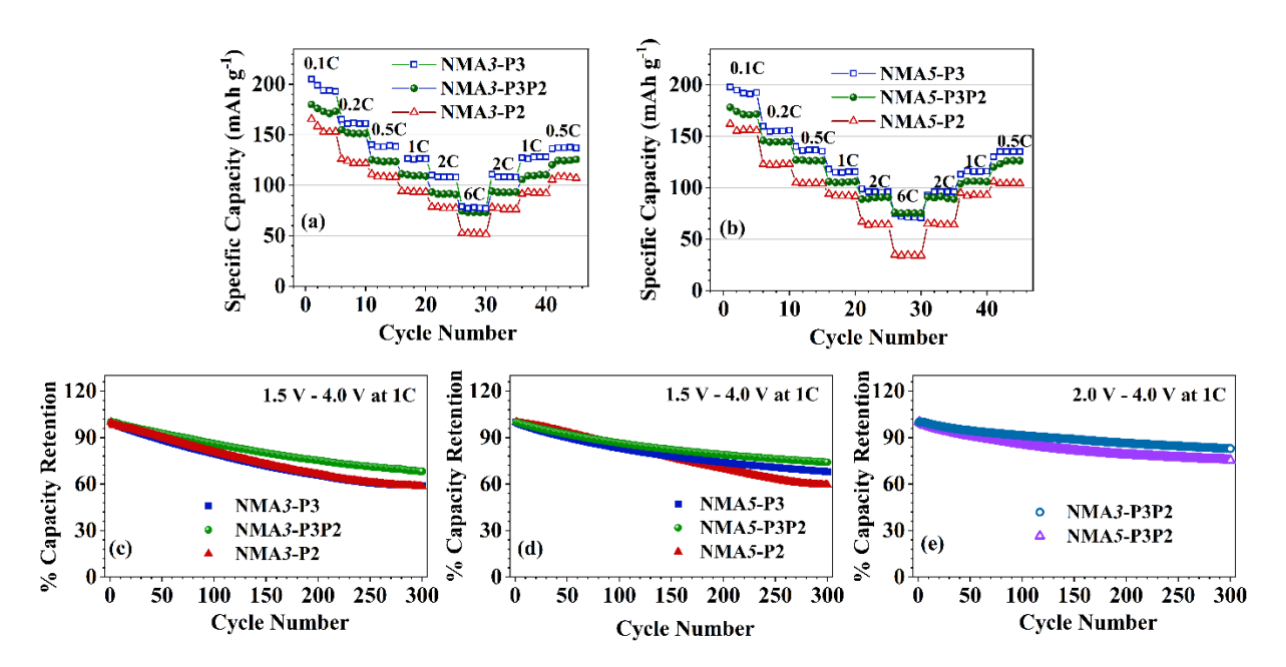


Fig. 7. Rate performance (a)-(b) and (c)-(d) cyclic stability curves of NMA3 and NMA5 series of cathodes cycled between 1.5 V and 4.0 V. (e) Cyclic performance of NMA3-P3P2 and NMA5-P3P2 at 1C between 2.0 V and 4.0 V.

To limit the activation of Mn<sup>3+/4+</sup> redox couples, NMA3-P3P2 and NMA5-P3P2 were tested further in a narrower voltage window between 2.0 V and 4.0 V (Fig. 7(e)). NMA3-P3P2 and NMA5-P3P2 exhibited about 82% and 75% capacity retention after 300 cycles at 1C in this voltage window. Although the superior cyclic performance of the NMA3-P3P2 compared to NMA5-P3P2 could be attributed to the presence of Jahn-Teller active Mn<sup>3+</sup> in the latter, the enhancement of cyclic stabilities of the cathode materials in the narrower voltage range is evidence of the detrimental impact (on cyclic stability) of utilizing Mn<sup>3+/4+</sup> redox couples in layered oxide cathodes.

Nyquist plots of half-cells with NMA3-P3P2 and NMA5-P3P2 samples as cathodes illustrated in Fig. S11 concur with the cyclic data. The Nyquist plot was analyzed through an equivalent circuit model shown in Fig. S11 inset. The circuit consists of 3 resistors, R1, R2, and R3, which represent the DC resistances of the electrolyte, SEI layers, and charge transfer, respectively.

Both NMA3-P3P2 and NMA5-P3P2 cells show higher overall resistance after cycling between 1.5-4.0 V when compared to the resistance of the cells cycled in 2.0-4.0 V range. In NMA3-P3P2, there was a drastic increase in the charge transfer resistance (R2) (60 to 350  $\Omega$ ) after cycling between 1.5-4.0 V compared to 2.0-4.0 V (60 to 150  $\Omega$ ) NMA5-P3P2 also exhibited similar trends in charge transfer resistance which is consistent with a higher degree of structural degradation in the cathodes cycled between 1.5-4.0 V.

# 3.3. Operando Synchrotron XRD

Operando Synchrotron XRD (SXRD) was used to probe variations in lattice parameters during cycling and investigate the structural variations in the cathode materials during cycling. Fig. 8(a-b) illustrates the operando SXRD pattern of NMA3-P3P2 and NMA5-P3P2 samples obtained at different states of charge. As expected, the figure shows large changes in the c lattice parameter of the P3 and P2 type unit cells below 2 V in both the cathodes, indicated by the significant shift in the (003) and (002) peaks of the P3 and P2 type phases. As discussed earlier, the change in the c lattice parameter is due to the presence of Jahn-Teller active Mn<sup>3+</sup>, which causes large distortions in the hexagonal lattice, leading to poor cyclic stability in the monophasic cathodes.

Interestingly, as reported in NMA2, the presence of Al<sup>3+</sup> in the NMA3 and NMA5 cathodes has also impeded the transformation of P3 phases into an O3-type structure at lower voltages. Even when the specific capacity of the cathodes reached as high as 190 mAh g<sup>-1</sup>, no peaks corresponding to the O3 phase were observed in both mixed-phase cathodes. P3 to O3 phase transformations have long been observed in P3 and O3-type materials. The slab glide mechanism leading to this transformation is often believed to cause rapid capacity degradation in these materials. Such transformations were also observed in NMA1-P3 and NMA1-P3P2 materials, which limited their cyclic performances [35, 47]. The absence of P3 to O3

transformations in both the Al-substituted compounds is an important finding and could open new avenues for research into O3 and P3-type layered oxides. The absence of phase transitions and the synergistic effect due to the biphasic nature of the NMA3-P3P2 and NMA5-P3P2 cathodes enhanced their structural stability, allowing them to achieve excellent cyclic properties.

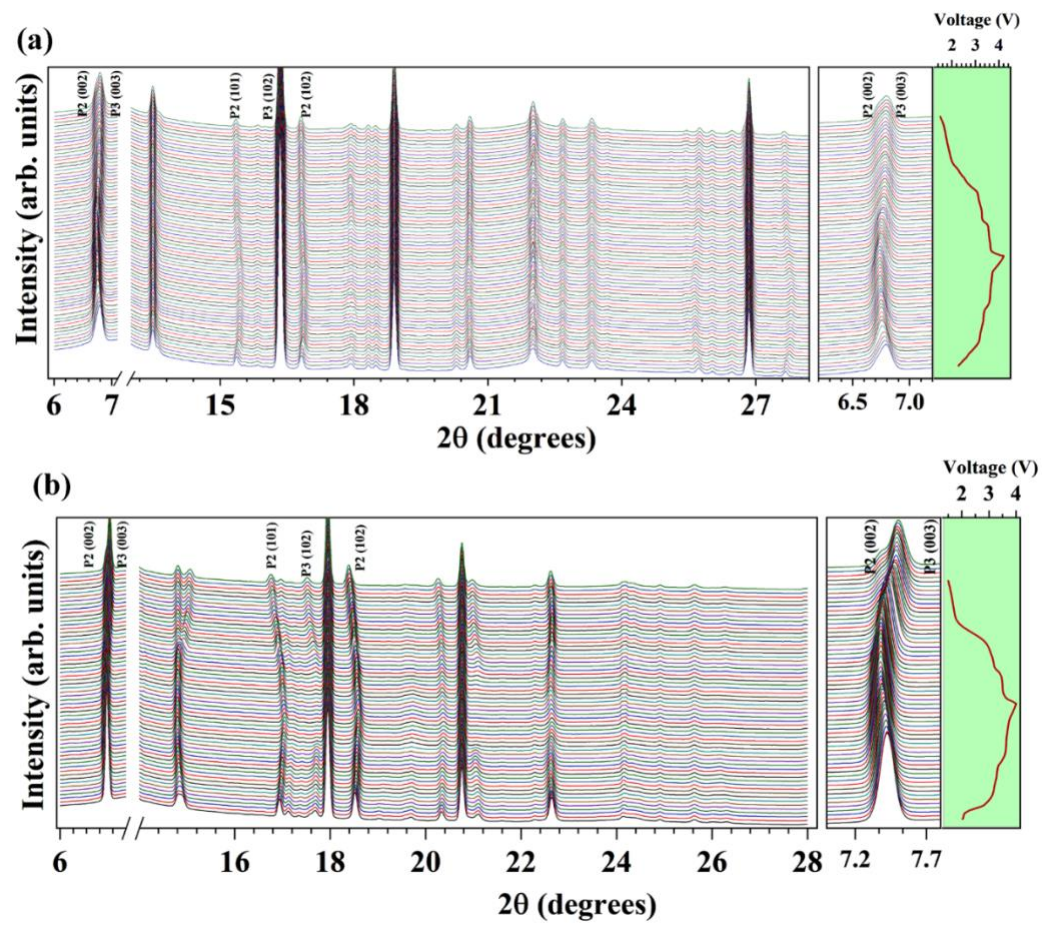


Fig. 8. *Operando* Synchrotron XRD patterns (a) NMA3-P3P2 (collected with a beam of wavelength of 0.6645 Å) and (b) NMA5-P3P2 (collected with a beam of wavelength of 0.74 Å) half cells obtained during the first charge/discharge cycle at 0.1C.

Fig. S12 classifies the compositions in the NMAx series along different Mn<sup>3+</sup> concentration lines in the Na<sub>3/4</sub>(Mn-Al-Ni)O<sub>2</sub> pseudo-ternary diagram and reveals some interesting trends. Along the constant Al content (= 0.25) from NMAx to NMAx, both the specific capacity and rate performance increased. This was expected as the Ni<sup>2+</sup> concentration in these cathode

materials increased from 0 (for NMA2) to 0.25 (NMA3), the amount of Na<sup>+</sup> that could be extracted also increased. This is further evidenced by almost similar specific capacities observed in NMA1, NMA5, and NMA3 cathodes having the same Ni content. The rate performance, on the other hand, improved along this line from NMA1 to NMA3. This is attributed to the increase in the Na<sup>+</sup> conduction bottleneck area with an increase in Al content from NMA1 to NMA3. Further, NMA3 and NMA5 compositions that exhibit the best rate performance and highest cyclic stability lie along the 0-Mn<sup>3+</sup> and 0.125-Mn<sup>3+</sup> lines, respectively. In a limited voltage window between 2.0 to 4.0 V, where the Mn<sup>3+/4+</sup> redox couple is largely inactive, NMA3-P3P2 showed better cyclic performance. Hence, the various Mn<sup>3+</sup> concentration lines displayed in Fig. S12 could serve as a guide to identify an optimal cathode material in the Na<sub>3/4</sub>(Mn-Al-Ni)O<sub>2</sub> pseudo-ternary diagram.

It should be noted that while Mn is +4 oxidation state in as-synthesized NMA3, during discharging to lower voltages in a half-cell configuration, sodiation could activate the Mn<sup>4+/3+</sup> redox due to additional Na-ions supplied by the Na metal anode. In the wider 1.5 V – 4.0 V window, NMA3-P3P2 and NMA5-P3P2 cathodes exhibited a 30% higher specific capacity than that in the 2.0 V – 4.0 V window while still retaining 70% of their initial specific capacity after 300 cycles. This cyclic performance points to excellent structural stabilities of NMA3-P3P2 and NMA5-P3P2 enabled by the presence of Al<sup>3+</sup> and their biphasic nature, which mitigate the effects of the structural distortions caused by the presence of Mn<sup>3+</sup>. Therefore, it stands to reason that an optimal cathode composition in the Na<sub>3/4</sub>(Mn-Al-Ni)O<sub>2</sub> pseudo-ternary diagram may be found along the lower Mn<sup>3+</sup> concentration line; however, the activation of Mn<sup>3+/4+</sup> redox couple could still be utilized to improve the electrochemical behavior while maintaining the structural stability of these cathodes.

# 4.0. Conclusions

A series of Al-substituted cathodes with different concentrations of Al, Mn, and Ni ions belonging to the Na<sub>3/4</sub>(Mn-Al-Ni) O<sub>2</sub> pseudo-ternary system was investigated. The compounds were synthesized in three-phase configurations by controlling the calcination temperature: monophasic P3, biphasic P3/P2, and monophasic P2. The varying proportions of Mn<sup>3+</sup> and Mn<sup>4+</sup> in the prepared cathode materials were quantified by analyzing their Mn 2p XPS spectra. P3-type cathodes with high Ni content exhibited capacities close to 195 mAh g<sup>-1</sup> and 75 mAh g<sup>-1</sup>, at 0.1C and 6C, respectively, between 1.5 to 4.0 V. The concentration of Mn<sup>3+</sup> and the biphasic nature of the materials were found to have a direct bearing on the cyclic performance of the cathode materials, enabling P3/P2 biphasic Na<sub>0.75</sub>Mn<sub>0.50</sub>Ni<sub>0.25</sub>Al<sub>0.25</sub>O<sub>2</sub> with no Mn<sup>3+</sup> to retain 70% of its original specific capacity after 300 cycles at 1C between 1.5-4.0 V. The capacity retention improved to 82% after the voltage window was limited to 2.0-4.0 V. The analysis of *operando* synchrotron XRD showed a large variation in the P3 and P2 unit cells during cycling below 2 V due to the activation of Mn<sup>3+/4+</sup> redox couples. This data also revealed the absence of P3 to O3 phase transformations in the Al-substituted samples, which may have aided in boosting their cyclic stability.

# Acknowledgments

SK thanks the Science and Engineering Research Board (SERB), Govt. of India, for the financial support (grant number: CRG/2021/005548).

# **Declaration of Interest**

The authors declare no conflict of interest.

# References

- [1] J.-M. Tarascon, Na-ion versus Li-ion Batteries: Complementarity Rather than Competitiveness, Joule, 4 (2020) 1616-1620 https://doi.org/10.1016/j.joule.2020.06.003.
- [2] T. Ahmad, D. Zhang, A critical review of comparative global historical energy consumption and future demand: The story told so far, Energy Rep., 6 (2020) 1973-1991 https://doi.org/10.1016/j.egyr.2020.07.020.
- [3] E. Goikolea, V. Palomares, S. Wang, I.R. de Larramendi, X. Guo, G. Wang, T. Rojo, Na-Ion Batteries—Approaching Old and New Challenges, Adv. Energy Mater., 10 (2020) 2002055 https://doi.org/10.1002/aenm.202002055.
- [4] R. Usiskin, Y. Lu, J. Popovic, M. Law, P. Balaya, Y.-S. Hu, J. Maier, Fundamentals, status and promise of sodium-based batteries, Nature Rev. Mater., 6 (2021) 1020-1035 https://doi.org/10.1038/s41578-021-00324-w.
- [5] R.J. Clément, P.G. Bruce, C.P. Grey, Review—Manganese-Based P2-Type Transition Metal Oxides as Sodium-Ion Battery Cathode Materials, J. Electrochem. Soc., 162 (2015) A2589-A2604 <a href="https://doi.org/10.1149/2.0201514jes">https://doi.org/10.1149/2.0201514jes</a>.
- [6] J. Darga, J. Lamb, A. Manthiram, Industrialization of Layered Oxide Cathodes for Lithium-Ion and Sodium-Ion Batteries: A Comparative Perspective, Energy Technol., 8 (2020) 2000723 <a href="https://doi.org/10.1002/ente.202000723">https://doi.org/10.1002/ente.202000723</a>.
- [7] Y. Tian, G. Zeng, A. Rutt, T. Shi, H. Kim, J. Wang, J. Koettgen, Y. Sun, B. Ouyang, T. Chen, Z. Lun, Z. Rong, K. Persson, G. Ceder, Promises and Challenges of Next-Generation "Beyond Li-ion" Batteries for Electric Vehicles and Grid Decarbonization, Chem. Rev., 121 (2021) 1623-1669 <a href="https://doi.org/10.1021/acs.chemrev.0c00767">https://doi.org/10.1021/acs.chemrev.0c00767</a>.

- [8] A. Patel, R. Mishra, R.K. Tiwari, A. Tiwari, D. Meghnani, S.K. Singh, R.K. Singh, Sustainable and efficient energy storage: A sodium ion battery anode from Aegle marmelos shell biowaste, J. Energy Storage, 72 (2023) 108424

  https://doi.org/10.1016/j.est.2023.108424.
- [9] M. Jiang, G. Qian, X.-Z. Liao, Z. Ren, Q. Dong, D. Meng, G. Cui, S. Yuan, S.-J. Lee, T. Qin, X. Liu, Y. Shen, Y.-S. He, L. Chen, Y. Liu, L. Li, Z.-F. Ma, Revisiting the capacity-fading mechanism of P2-type sodium layered oxide cathode materials during high-voltage cycling, J. Energy Chem., 69 (2022) 16-25 <a href="https://doi.org/10.1016/j.jechem.2022.01.010">https://doi.org/10.1016/j.jechem.2022.01.010</a>. [10] Z. Liu, X. Xu, S. Ji, L. Zeng, D. Zhang, J. Liu, Recent Progress of P2-Type Layered Transition-Metal Oxide Cathodes for Sodium-Ion Batteries, Chem. Eur. J., 26 (2020) 7747-7766 <a href="https://doi.org/10.1002/chem.201905131">https://doi.org/10.1002/chem.201905131</a>.
- [11] L. Xu, Q. Ran, L. Li, Q. Hu, G. Cai, X. Liu, A multiphase coupling strategy to structurally stable manganese-based oxides cathode for high electrochemical performance sodium ion batteries, Electrochim. Acta, 467 (2023) 143085

  <a href="https://doi.org/10.1016/j.electacta.2023.143085">https://doi.org/10.1016/j.electacta.2023.143085</a>.
- [12] J. Xiao, X. Li, K. Tang, D. Wang, M. Long, H. Gao, W. Chen, C. Liu, H. Liu, G. Wang, Recent progress of emerging cathode materials for sodium ion batteries, Materials Chemistry Frontiers, 5 (2021) 3735-3764 10.1039/D1QM00179E.
- [13] M. He, S. Liu, J. Wu, J. Zhu, Review of cathode materials for sodium-ion batteries, Prog. Solid State Chem., (2024) 100452 <a href="https://doi.org/10.1016/j.progsolidstchem.2024.100452">https://doi.org/10.1016/j.progsolidstchem.2024.100452</a>.
- [14] Y. Gupta, P. Siwatch, R. Karwasra, K. Sharma, S.K. Tripathi, Recent progress of layered structured P2- and O3- type transition metal oxides as cathode material for sodium-ion batteries, Renew. Sust. Energ. Rev., 192 (2024) 114167

https://doi.org/10.1016/j.rser.2023.114167.

[15] V. Palomares, P. Serras, I. Villaluenga, K.B. Hueso, J. Carretero-González, T. Rojo, Naion batteries, recent advances and present challenges to become low cost energy storage systems, Energy Environ. Sci., 5 (2012) 5884-5901 <a href="https://doi.org/10.1039/C2EE02781J">https://doi.org/10.1039/C2EE02781J</a>. [16] P.-F. Wang, Y. You, Y.-X. Yin, Y.-G. Guo, Layered Oxide Cathodes for Sodium-Ion Batteries: Phase Transition, Air Stability, and Performance, Adv. Energy Mater., 8 (2018) 1701912 <a href="https://doi.org/10.1002/aenm.201701912">https://doi.org/10.1002/aenm.201701912</a>.

[17] F. Wei, Q. Zhang, P. Zhang, W. Tian, K. Dai, L. Zhang, J. Mao, G. Shao, Review—Research Progress on Layered Transition Metal Oxide Cathode Materials for Sodium Ion Batteries, J. Electrochem. Soc., 168 (2021) 050524 <a href="https://doi.org/10.1149/1945-7111/abf9bf">https://doi.org/10.1149/1945-7111/abf9bf</a>. [18] C. Delmas, C. Fouassier, P. Hagenmuller, Structural classification and properties of the layered oxides, Physica B+C, 99 (1980) 81-85 <a href="https://doi.org/10.1016/0378-4363(80)90214-4">https://doi.org/10.1016/0378-4363(80)90214-4</a>.

[19] R. Mishra, S.K. Singh, H. Gupta, N. Srivastava, D. Meghnani, R.K. Tiwari, A. Patel, A. Tiwari, V.K. Tiwari, R.K. Singh, Surface modification of nano Na[Ni<sub>0.60</sub>Mn<sub>0.35</sub>Co<sub>0.05</sub>]O<sub>2</sub> cathode material by dextran functionalized RGO via hydrothermal treatment for high performance sodium batteries, Appl. Surf. Sci., 535 (2021) 147695 https://doi.org/10.1016/j.apsusc.2020.147695.

[20] Z.-Y. Li, R. Gao, L. Sun, Z. Hu, X. Liu, Zr-doped P2-

Na<sub>0.75</sub>Mn<sub>0.55</sub>Ni<sub>0.25</sub>Co<sub>0.05</sub>Fe<sub>0.10</sub>Zr<sub>0.05</sub>O<sub>2</sub> as high-rate performance cathode material for sodium ion batteries, Electrochim. Acta, 223 (2017) 92-99 https://doi.org/10.1016/j.electacta.2016.12.019.

[21] D. Yuan, X. Hu, J. Qian, F. Pei, F. Wu, R. Mao, X. Ai, H. Yang, Y. Cao, P2-type Na<sub>0.67</sub>Mn<sub>0.65</sub>Fe<sub>0.2</sub>Ni<sub>0.15</sub>O<sub>2</sub> Cathode Material with High-capacity for Sodium-ion Battery, Electrochim. Acta, 116 (2014) 300-305 <a href="https://doi.org/10.1016/j.electacta.2013.10.211">https://doi.org/10.1016/j.electacta.2013.10.211</a>.

- [22] P. Manikandan, D. Ramasubramonian, M.M. Shaijumon, Layered P2-type Na<sub>0.5</sub>Ni<sub>0.25</sub>Mn<sub>0.75</sub>O<sub>2</sub> as a high performance cathode material for sodium-ion batteries, Electrochim. Acta, 206 (2016) 199-206 <a href="https://doi.org/10.1016/j.electacta.2016.04.138">https://doi.org/10.1016/j.electacta.2016.04.138</a>.
- [23] H.N. Vasavan, M. Badole, S. Saxena, A.K. Das, S. Deswal, P. Kumar, S. Kumar, Excellent Structural Stability-Driven Cyclability in P2-Type Ti-Based Cathode for Na-Ion Batteries, ACS Appl. Energy Mater., 6 (2023) 2440-2447

  <a href="https://doi.org/10.1021/acsaem.2c03750">https://doi.org/10.1021/acsaem.2c03750</a>.
- [24] H.N. Vasavan, M. Badole, S. Dwivedi, S. Kumar, Structural and transport properties of P2-Type Na<sub>0.70</sub>Ni<sub>0.20</sub>Cu<sub>0.15</sub>Mn<sub>0.65</sub>O<sub>2</sub> layered oxide, Ceram. Int., 48 (2022) 28986-28993 https://doi.org/10.1016/j.ceramint.2022.04.206.
- [25] G. Liu, W. Xu, J. Wu, Y. Li, L. Chen, S. Li, Q. Ren, J. Wang, Unlocking high-rate O3 layered oxide cathode for Na-ion batteries via ion migration path modulation, J. Energy Chem., 83 (2023) 53-61 <a href="https://doi.org/10.1016/j.jechem.2023.04.029">https://doi.org/10.1016/j.jechem.2023.04.029</a>.
- [26] X. Li, X. Shen, J. Zhao, Y. Yang, Q. Zhang, F. Ding, M. Han, C. Xu, C. Yang, H. Liu, Y.-S. Hu, O3-NaFe<sub>(1/3-x)</sub>Ni<sub>1/3</sub>Mn<sub>1/3</sub>Al<sub>x</sub>O<sub>2</sub> Cathodes with Improved Air Stability for Na-Ion Batteries, ACS Appl. Mater. Interfaces, 13 (2021) 33015-33023 https://doi.org/10.1021/acsami.1c07554.
- [27] L. Yu, Y.-X. Chang, M. Liu, Y.-H. Feng, D. Si, X. Zhu, X.-Z. Wang, P.-F. Wang, S. Xu, O3-Type Na<sub>0.95</sub>Ni<sub>0.40</sub>Fe<sub>0.15</sub>Mn<sub>0.3</sub>Ti<sub>0.15</sub>O<sub>2</sub> Cathode Materials with Enhanced Storage Stability for High-Energy Na-Ion Batteries, ACS Appl. Mater. Interfaces, 15 (2023) 23236-23245 <a href="https://doi.org/10.1021/acsami.3c02514">https://doi.org/10.1021/acsami.3c02514</a>.
- [28] R. Li, Y. Liu, Z. Wang, J. Li, A P2/O3 biphasic cathode material with highly reversibility synthesized by Sn-substitution for Na-ion batteries, Electrochim. Acta, 318 (2019) 14-22 <a href="https://doi.org/10.1016/j.electacta.2019.06.020">https://doi.org/10.1016/j.electacta.2019.06.020</a>.

- [29] S. Saxena, H.N. Vasavan, M. Badole, A.K. Das, S. Deswal, P. Kumar, S. Kumar, Tailored P2/O3 phase-dependent electrochemical behavior of Mn-based cathode for sodiumion batteries, J. Energy Storage, 64 (2023) 107242 <a href="https://doi.org/10.1016/j.est.2023.107242">https://doi.org/10.1016/j.est.2023.107242</a>.
- [30] L. Yang, J.M.L. del Amo, Z. Shadike, S.-M. Bak, F. Bonilla, M. Galceran, P.K. Nayak, J.R. Buchheim, X.-Q. Yang, T. Rojo, P. Adelhelm, A Co- and Ni-Free P2/O3 Biphasic Lithium Stabilized Layered Oxide for Sodium-Ion Batteries and its Cycling Behavior, Adv. Funct. Mater., 30 (2020) 2003364 <a href="https://doi.org/10.1002/adfm.202003364">https://doi.org/10.1002/adfm.202003364</a>.
- [31] E. Lee, J. Lu, Y. Ren, X. Luo, X. Zhang, J. Wen, D. Miller, A. DeWahl, S. Hackney, B. Key, D. Kim, M.D. Slater, C.S. Johnson, Layered P2/O3 Intergrowth Cathode: Toward High Power Na-Ion Batteries, Adv. Energy Mater., 4 (2014) 1400458

  <a href="https://doi.org/10.1002/aenm.201400458">https://doi.org/10.1002/aenm.201400458</a>.
- [32] X. Liang, T.-Y. Yu, H.-H. Ryu, Y.-K. Sun, Hierarchical O3/P2 heterostructured cathode materials for advanced sodium-ion batteries, Energy Storage Mater., 47 (2022) 515-525 https://doi.org/10.1016/j.ensm.2022.02.043.
- [33] S. Saxena, M. Badole, H.N. Vasavan, V. Srihari, A.K. Das, P. Gami, S. Deswal, P. Kumar, S. Kumar, Deciphering the role of optimal P2/O3 phase fraction in enhanced cyclability and specific capacity of layered oxide cathodes, Chem. Eng. J., 485 (2024) 149921 <a href="https://doi.org/10.1016/j.cej.2024.149921">https://doi.org/10.1016/j.cej.2024.149921</a>.
- [34] C. Hakim, H.D. Asfaw, R. Younesi, D. Brandell, K. Edström, I. Saadoune, Development of P2 or P2/P3 cathode materials for sodium-ion batteries by controlling the Ni and Mn contents in Na<sub>0.7</sub>Co<sub>x</sub>Mn<sub>y</sub>Ni<sub>z</sub>O<sub>2</sub> layered oxide, Electrochim. Acta, 438 (2023) 141540 <a href="https://doi.org/10.1016/j.electacta.2022.141540">https://doi.org/10.1016/j.electacta.2022.141540</a>.
- [35] H.N. Vasavan, M. Badole, S. Saxena, V. Srihari, A.K. Das, P. Gami, S. Deswal, P. Kumar, S. Kumar, Impact of P3/P2 mixed phase on the structural and electrochemical

performance of Na<sub>0.75</sub>Mn<sub>0.75</sub>Al<sub>0.25</sub>O<sub>2</sub> cathode, J. Energy Storage, 74 (2023) 109428 https://doi.org/10.1016/j.est.2023.109428.

- [36] J. Feng, D. Fang, Z. Yang, J. Zhong, C. Zheng, Z. Wei, J. Li, A novel P2/O3 composite cathode toward synergistic electrochemical optimization for sodium ion batteries, J. Power Sources, 553 (2023) 232292 https://doi.org/10.1016/j.jpowsour.2022.232292.
- [37] X. Wu, G.-L. Xu, G. Zhong, Z. Gong, M.J. McDonald, S. Zheng, R. Fu, Z. Chen, K. Amine, Y. Yang, Insights into the Effects of Zinc Doping on Structural Phase Transition of P2-Type Sodium Nickel Manganese Oxide Cathodes for High-Energy Sodium Ion Batteries, ACS Appl. Mater. Interfaces, 8 (2016) 22227-22237 https://doi.org/10.1021/acsami.6b06701.
- [38] H.N. Vasavan, M. Badole, S. Dwivedi, D. Kumar, P. Kumar, S. Kumar, Enhanced rate performance and specific capacity in Ti-substituted P2-type layered oxide enabled by crystal structure and particle morphology modifications, Chem. Eng. J., 448 (2022) 137662 <a href="https://doi.org/10.1016/j.cej.2022.137662">https://doi.org/10.1016/j.cej.2022.137662</a>.
- [39] W.-L. Pang, X.-H. Zhang, J.-Z. Guo, J.-Y. Li, X. Yan, B.-H. Hou, H.-Y. Guan, X.-L. Wu, P2-type Na<sub>2/3</sub>Mn<sub>1-x</sub>Al<sub>x</sub>O<sub>2</sub> cathode material for sodium-ion batteries: Al-doped enhanced electrochemical properties and studies on the electrode kinetics, J. Power Sources, 356 (2017) 80-88 <a href="https://doi.org/10.1016/j.jpowsour.2017.04.076">https://doi.org/10.1016/j.jpowsour.2017.04.076</a>.
- [40] X. Wu, J. Guo, D. Wang, G. Zhong, M.J. McDonald, Y. Yang, P2-type Na<sub>0.66</sub>Ni<sub>0.33-</sub>xZn<sub>x</sub>Mn<sub>0.67</sub>O<sub>2</sub> as new high-voltage cathode materials for sodium-ion batteries, J. Power Sources, 281 (2015) 18-26 https://doi.org/10.1016/j.jpowsour.2014.12.083.
- [41] G. Singh, N. Tapia-Ruiz, J.M. Lopez del Amo, U. Maitra, J.W. Somerville, A.R. Armstrong, J. Martinez de Ilarduya, T. Rojo, P.G. Bruce, High Voltage Mg-Doped Na<sub>0.67</sub>Ni<sub>0.3-x</sub>Mg<sub>x</sub>Mn<sub>0.7</sub>O<sub>2</sub> (x = 0.05, 0.1) Na-Ion Cathodes with Enhanced Stability and Rate Capability, Chem. Mater., 28 (2016) 5087-5094 https://doi.org/10.1021/acs.chemmater.6b01935.

- [42] C. Santamaría, E. Morales, C.d. Rio, B. Herradón, J.M. Amarilla, Studies on sodium-ion batteries: Searching for the proper combination of the cathode material, the electrolyte and the working voltage. The role of magnesium substitution in layered manganese-rich oxides, and pyrrolidinium ionic liquid, Electrochim. Acta, 439 (2023) 141654

  <a href="https://doi.org/10.1016/j.electacta.2022.141654">https://doi.org/10.1016/j.electacta.2022.141654</a>.
- [43] A. Chakraborty, S. Kunnikuruvan, S. Kumar, B. Markovsky, D. Aurbach, M. Dixit, D.T. Major, Layered Cathode Materials for Lithium-Ion Batteries: Review of Computational Studies on LiNi<sub>1-x-y</sub>Co<sub>x</sub>Mn<sub>y</sub>O<sub>2</sub> and LiNi<sub>1-x-y</sub>Co<sub>x</sub>Al<sub>y</sub>O<sub>2</sub>, Chem. Mater., 32 (2020) 915-952 https://doi.org/10.1021/acs.chemmater.9b04066.
- [44] S.-T. Myung, F. Maglia, K.-J. Park, C.S. Yoon, P. Lamp, S.-J. Kim, Y.-K. Sun, Nickel-Rich Layered Cathode Materials for Automotive Lithium-Ion Batteries: Achievements and Perspectives, ACS Energy Lett., 2 (2017) 196-223 https://doi.org/10.1021/acsenergylett.6b00594.
- [45] A. Hebert, C. David, E. McCalla, Combinatorial Investigation of the Impact of Systematic Al Substitution into LiNi<sub>1-x-y</sub>Mn<sub>x</sub>Co<sub>y</sub>O<sub>2</sub> Materials, ACS Appl. Energy Mater., 6 (2023) 4593-4603 <a href="https://doi.org/10.1021/acsaem.2c03994">https://doi.org/10.1021/acsaem.2c03994</a>.
- [46] D. Meghnani, H. Gupta, S.K. Singh, N. Srivastava, R. Mishra, R.K. Tiwari, A. Patel, A. Tiwari, R.K. Singh, Enhanced Cyclic Stability of LiNi<sub>0.815</sub>Co<sub>0.15</sub>Al<sub>0.035</sub>O<sub>2</sub> Cathodes by Surface Modification with BiPO<sub>4</sub> for Applications in Rechargeable Lithium Polymer Batteries, ChemElectroChem, 8 (2021) 2867-2880 <a href="https://doi.org/10.1002/celc.202100629">https://doi.org/10.1002/celc.202100629</a>.
- [47] H.N. Vasavan, M. Badole, S. Saxena, V. Srihari, A.K. Das, P. Gami, S. Deswal, P. Kumar, S. Kumar, Unveiling the Potential of P3 Phase in Enhancing the Electrochemical Performance of a Layered Oxide Cathode, Mater. Today Energy., 37 (2023) 101380 https://doi.org/10.1016/j.mtener.2023.101380.

- [48] X. Liu, W. Zuo, B. Zheng, Y. Xiang, K. Zhou, Z. Xiao, P. Shan, J. Shi, Q. Li, G. Zhong, R. Fu, Y. Yang, P2-Na<sub>0.67</sub>Al<sub>x</sub>Mn<sub>1-x</sub>O<sub>2</sub>: Cost-Effective, Stable and High-Rate Sodium Electrodes by Suppressing Phase Transitions and Enhancing Sodium Cation Mobility, Angew. Chem. Int. Ed., 58 (2019) 18086-18095 <a href="https://doi.org/10.1002/anie.201911698">https://doi.org/10.1002/anie.201911698</a>.
- [49] A. Coelho, TOPAS and TOPAS-Academic: an optimization program integrating computer algebra and crystallographic objects written in C++, J. Appl. Crystallogr., 51 (2018) 210-218 <a href="https://doi.org/10.1107/S1600576718000183">https://doi.org/10.1107/S1600576718000183</a>.
- [50] S. Hüfner, Photoelectron spectroscopy: principles and applications, Springer Science & Business Media2013.
- [51] J.F. Moulder, J. Chastain, Handbook of X-ray Photoelectron Spectroscopy: A Reference Book of Standard Spectra for Identification and Interpretation of XPS Data, Physical Electronics Division, Perkin-Elmer Corporation1992.
- [52] W. Kang, D.Y.W. Yu, P.-K. Lee, Z. Zhang, H. Bian, W. Li, T.-W. Ng, W. Zhang, C.-S. Lee, P2-Type Na<sub>x</sub>Cu<sub>0.15</sub>Ni<sub>0.20</sub>Mn<sub>0.65</sub>O<sub>2</sub> Cathodes with High Voltage for High-Power and Long-Life Sodium-Ion Batteries, ACS Appl. Mater. Interfaces, 8 (2016) 31661-31668 <a href="https://doi.org/10.1021/acsami.6b10841">https://doi.org/10.1021/acsami.6b10841</a>.
- [53] Z. Zhang, R. Wang, J. Zeng, K. Shi, C. Zhu, X. Yan, Size Effects in Sodium Ion Batteries, Adv. Funct. Mater., 31 (2021) 2106047 <a href="https://doi.org/10.1002/adfm.202106047">https://doi.org/10.1002/adfm.202106047</a>.
- [54] V. Pamidi, S. Trivedi, S. Behara, M. Fichtner, M.A. Reddy, Micron-sized single-crystal cathodes for sodium-ion batteries, iScience, 25 (2022) 104205 https://doi.org/10.1016/j.isci.2022.104205.
- [55] Q. Pei, M. Lu, Z. Liu, D. Li, X. Rao, X. Liu, S. Zhong, Improving the Na<sub>0.67</sub>Ni<sub>0.33</sub>Mn<sub>0.67</sub>O<sub>2</sub> Cathode Material for High-Voltage Cyclability via Ti/Cu Codoping for

Sodium-Ion Batteries, ACS Appl. Energy Mater., 5 (2022) 1953-1962 https://doi.org/10.1021/acsaem.1c03466.

[56] L. Wang, Y.-G. Sun, L.-L. Hu, J.-Y. Piao, J. Guo, A. Manthiram, J. Ma, A.-M. Cao, Copper-substituted Na<sub>0.67</sub>Ni<sub>0.3-x</sub>Cu<sub>x</sub>Mn<sub>0.7</sub>O<sub>2</sub> cathode materials for sodium-ion batteries with suppressed P2–O2 phase transition, J. Mater. Chem. A, 5 (2017) 8752-8761 <a href="https://doi.org/10.1039/C7TA00880E">https://doi.org/10.1039/C7TA00880E</a>.

[57] R. Mishra, R.K. Tiwari, A. Patel, A. Tiwari, R.K. Singh, A twofold approach for prolonging the lifespan of cobalt-free Na[Ni<sub>0.55</sub>Mn<sub>0.35</sub>Fe<sub>0.1</sub>]O<sub>2</sub> cathode via Bi<sup>5+</sup>-doping and Bi<sub>2</sub>O<sub>3</sub> coating in sodium ion batteries, J. Energy Storage, 77 (2024) 110058 <a href="https://doi.org/10.1016/j.est.2023.110058">https://doi.org/10.1016/j.est.2023.110058</a>.

# [Supplementary Material]

# Rational Design of an Optimal Al-substituted Layered Oxide Cathode for Na-ion Batteries

Hari Narayanan Vasavan <sup>a</sup>, Manish Badole <sup>a</sup>, Samriddhi Saxena <sup>a</sup>, Velaga Srihari<sup>b</sup>, Asish Kumar Das <sup>a</sup>, Pratiksha Gami <sup>a</sup>, Neha Dagar <sup>a</sup>, Sonia Deswal <sup>c</sup>, Pradeep Kumar <sup>c</sup>, Himanshu Kumar Poswal <sup>b</sup>, and Sunil Kumar <sup>a,d,\*</sup>

<sup>a</sup> Department of Metallurgical Engineering and Materials Science, Indian Institute of Technology Indore, Simrol, 453552, India.

<sup>b</sup> High Pressure & Synchrotron Radiation Physics Division, Bhabha Atomic Research Centre, 400085 Mumbai, India

<sup>c</sup> School of Physical Sciences, Indian Institute of Technology Mandi, Himachal Pradesh, 175005, India

<sup>d</sup> Center for Electric Vehicle and Intelligent Transport Systems, Indian Institute of Technology Indore, Simrol, 453552, India.

\* Corresponding Author: sunil@iiti.ac.in

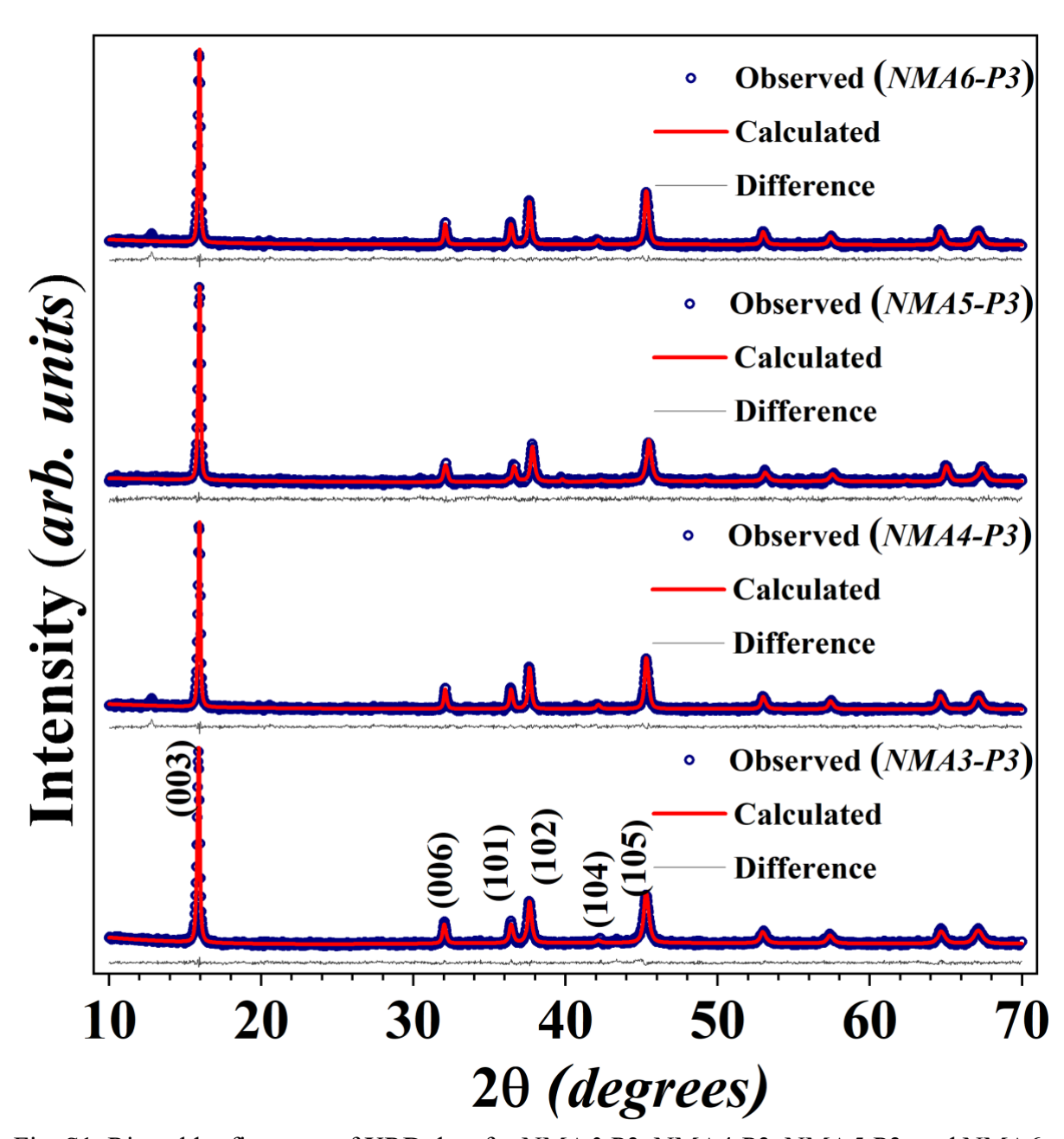


Fig. S1. Rietveld refinement of XRD data for NMA*3*-P3, NMA4-P3, NMA*5*-P3, and NMA6-P3 samples.

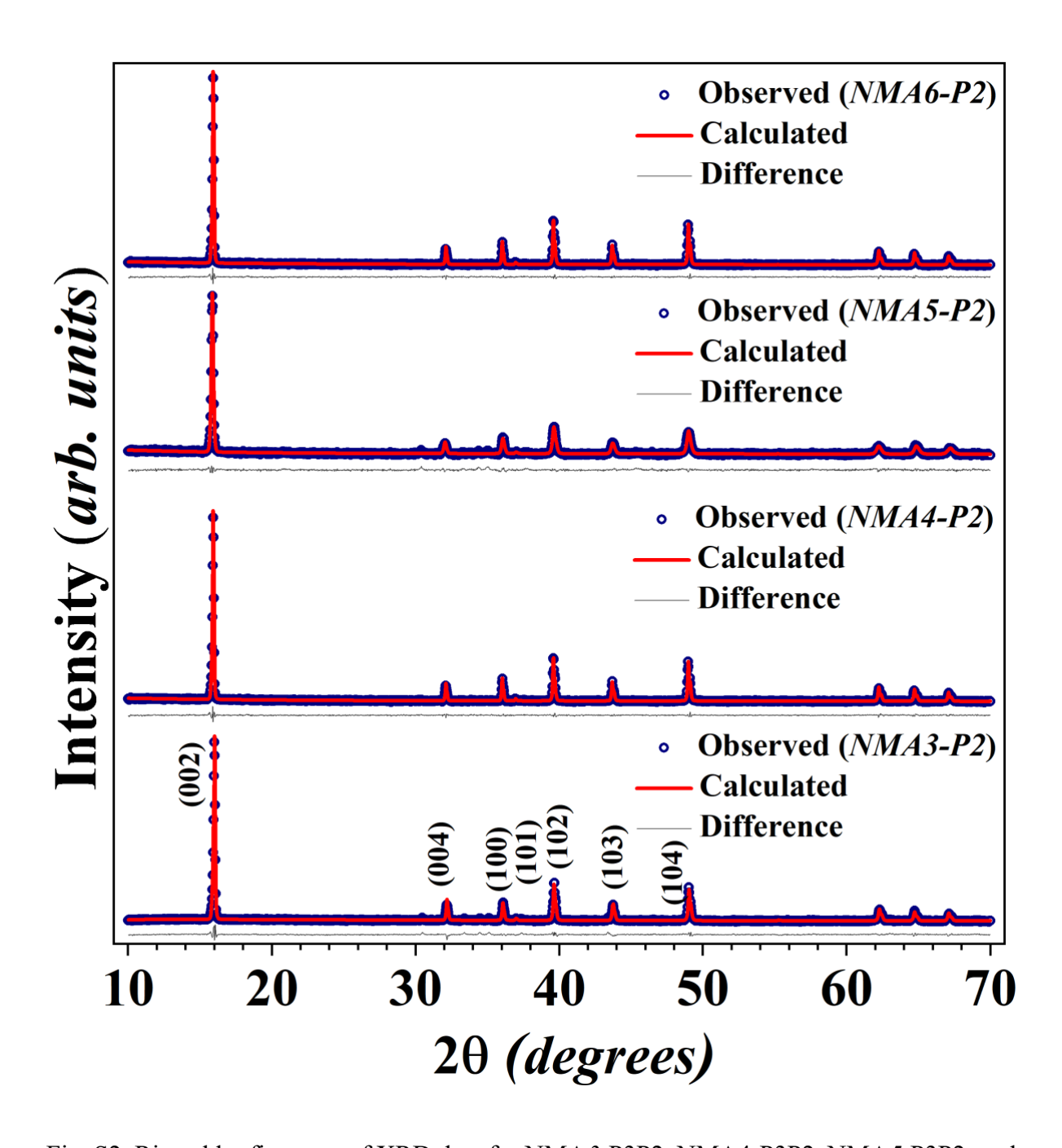


Fig. S2. Rietveld refinement of XRD data for NMA3-P3P2, NMA4-P3P2, NMA5-P3P2, and NMA6-P3P2 samples.

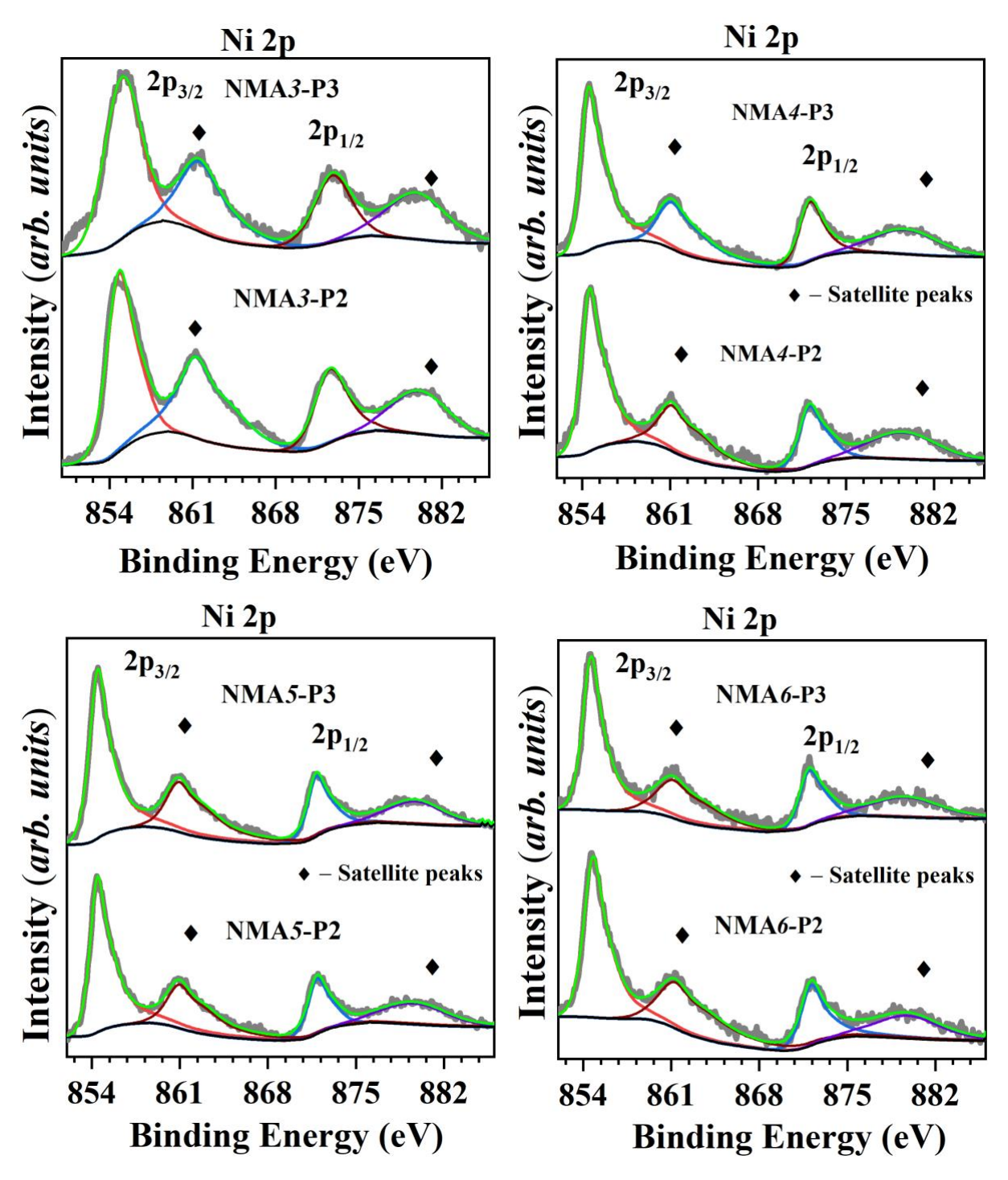


Fig. S3. Ni 2p XPS plots of NMAx-P3 and NMAx-P2 type samples.

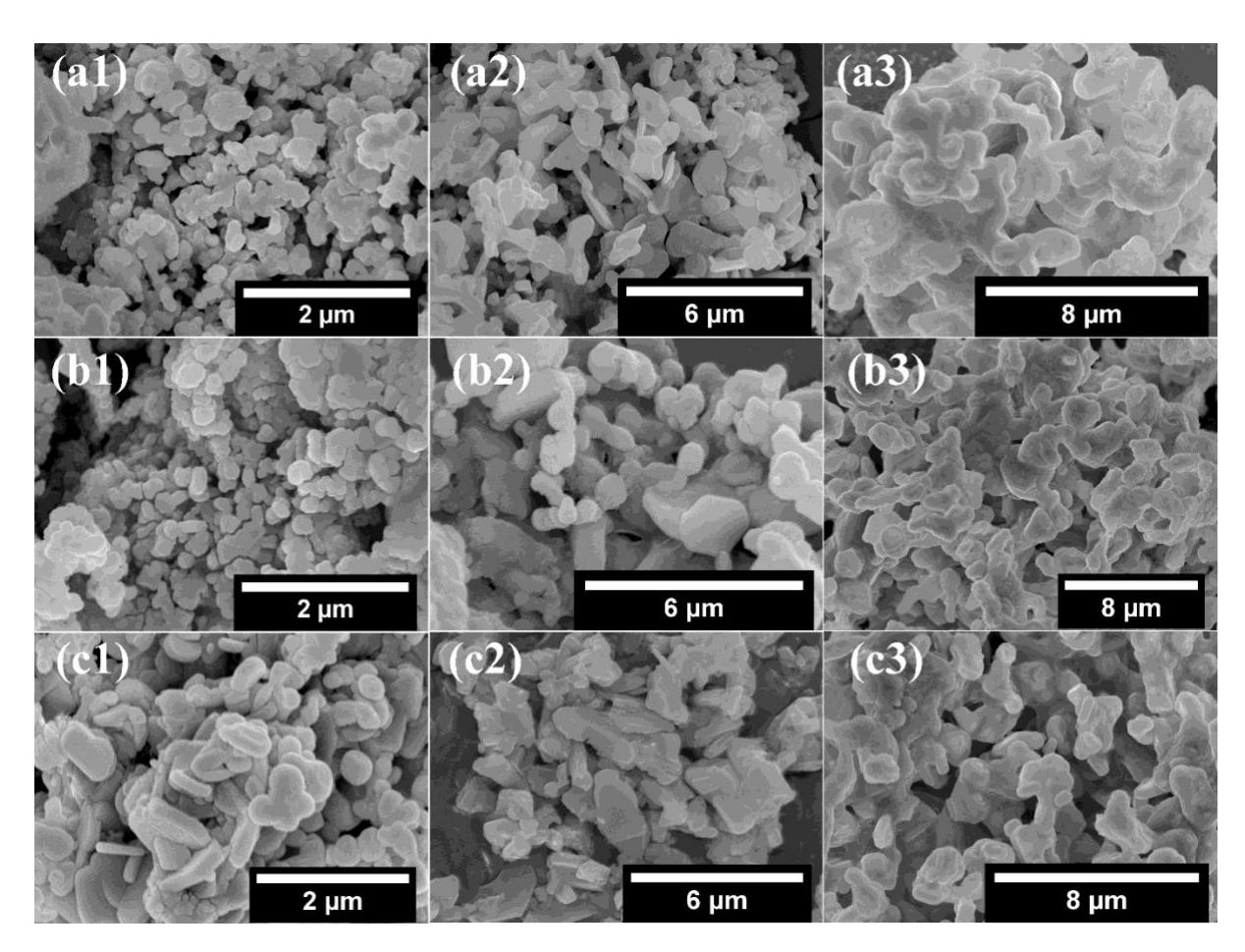


Fig. S4. SEM micrographs of (a1-a3) NMA3-P3, P3P2, and P2, respectively. (b1-b3) NMA4-P3, P3P2, and P2, respectively. (c1-c3) NMA6-P3, P3P2, and P2, respectively.

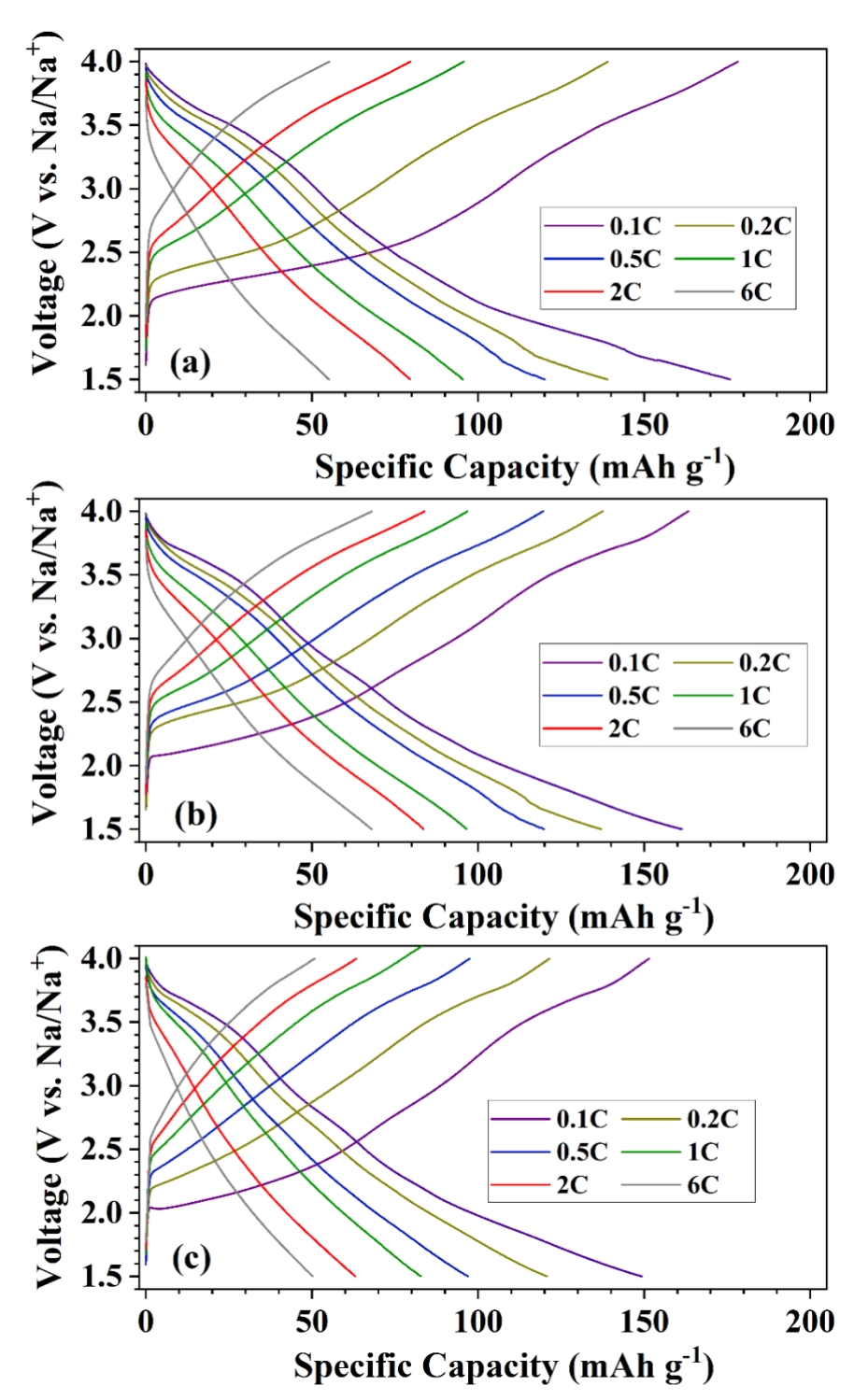


Fig. S5. Charge-discharge profiles of (a) NMA4-P3, (b) NMA4-P3P2, and (c) NMA4-P2 cathodes at different C rates.

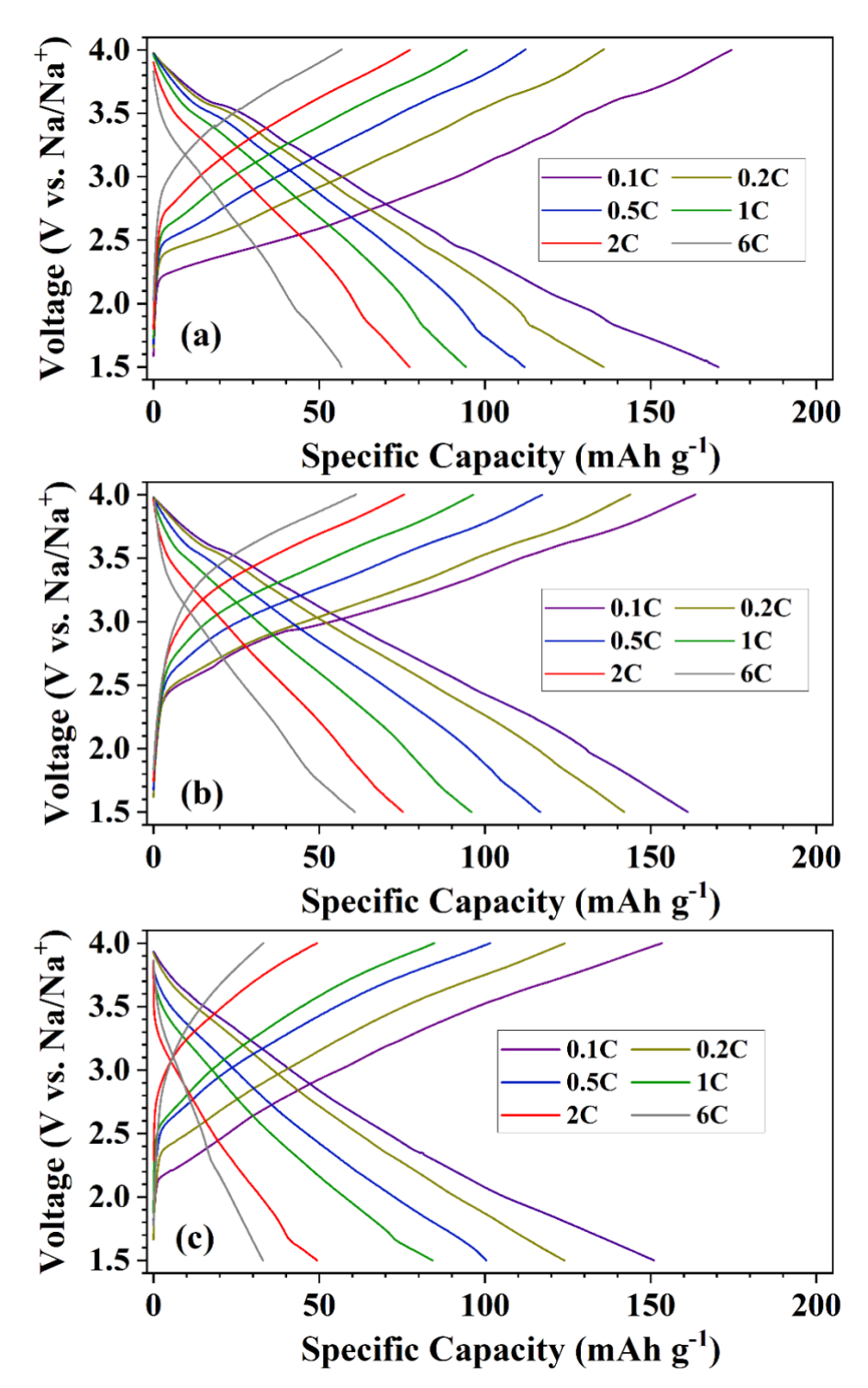


Fig. S6. Charge-discharge profiles of (a) NMA6-P3, (b) NMA6-P3P2, and (c) NMA6-P2 cathodes at different C rates.

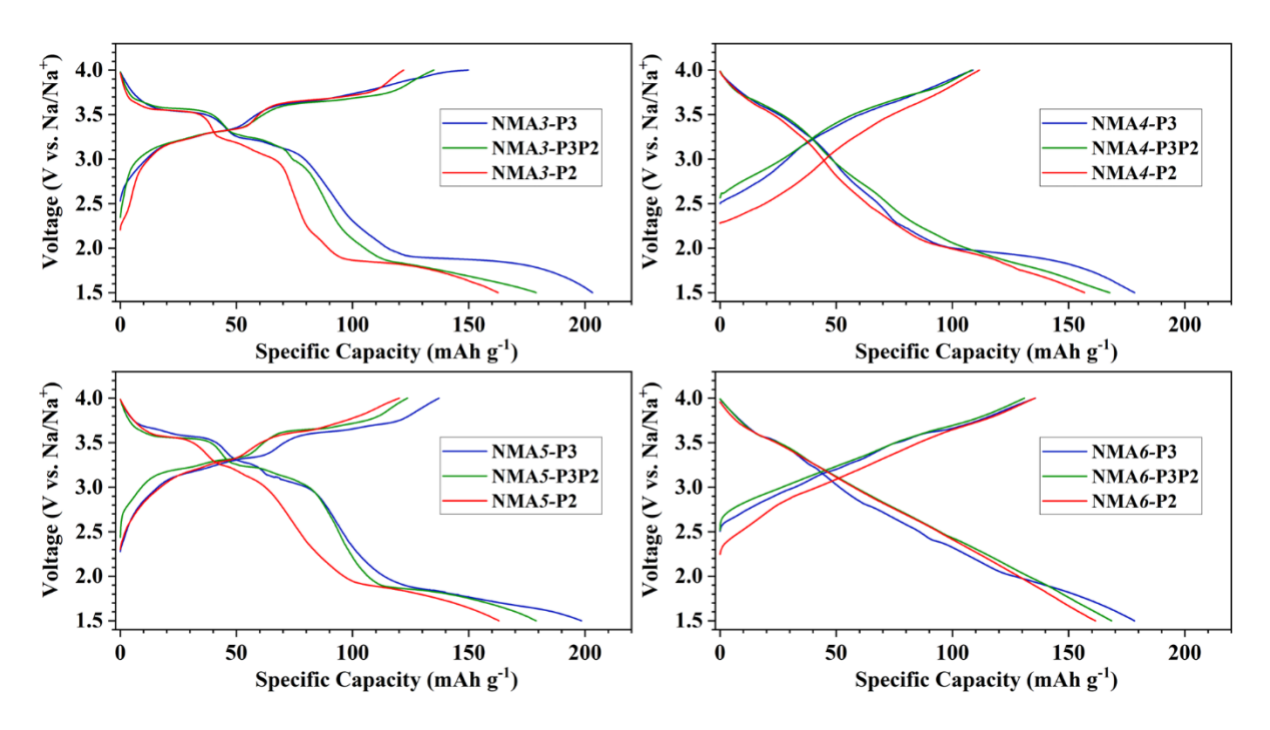


Fig. S7. GCD curves showing the first charge-discharge profiles of the NMAx series of samples at 0.1C.

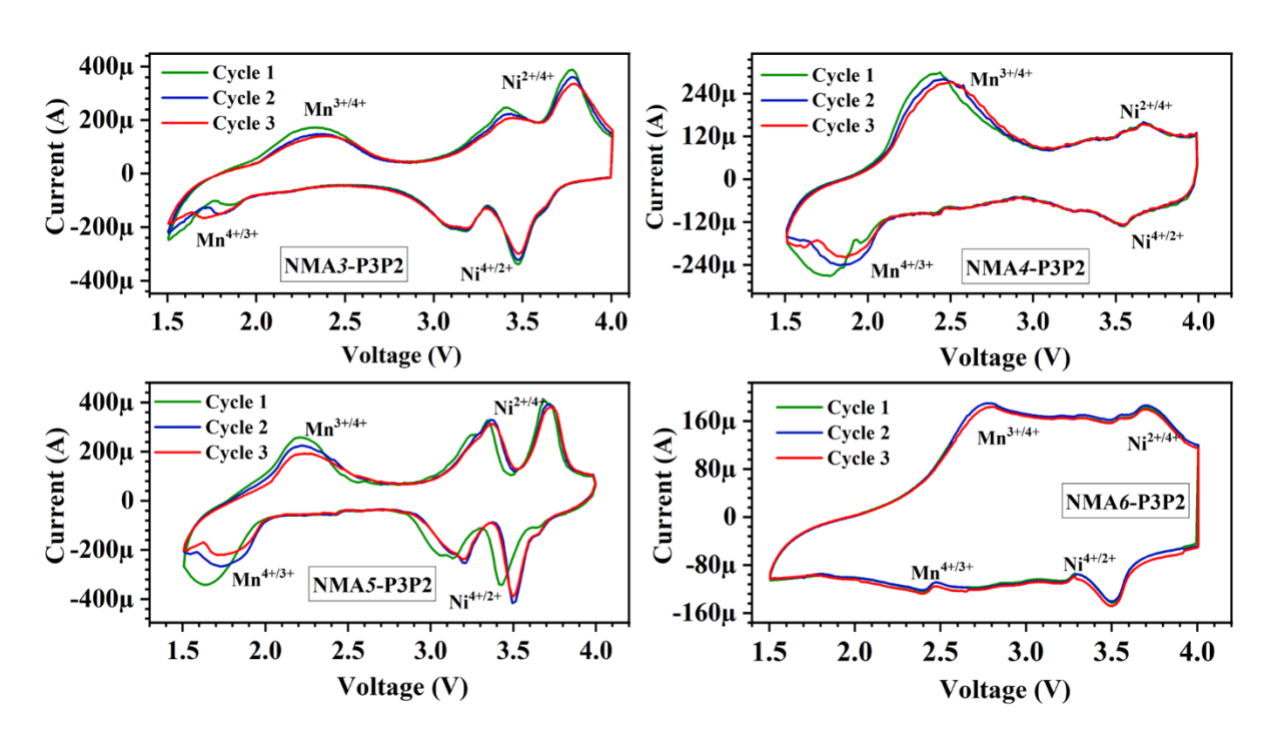


Fig. S8. CV curves of NMA3-P3P2, NMA4-P3P2, NMA5-P3P2 and NMA6-P3P2 cathodes.

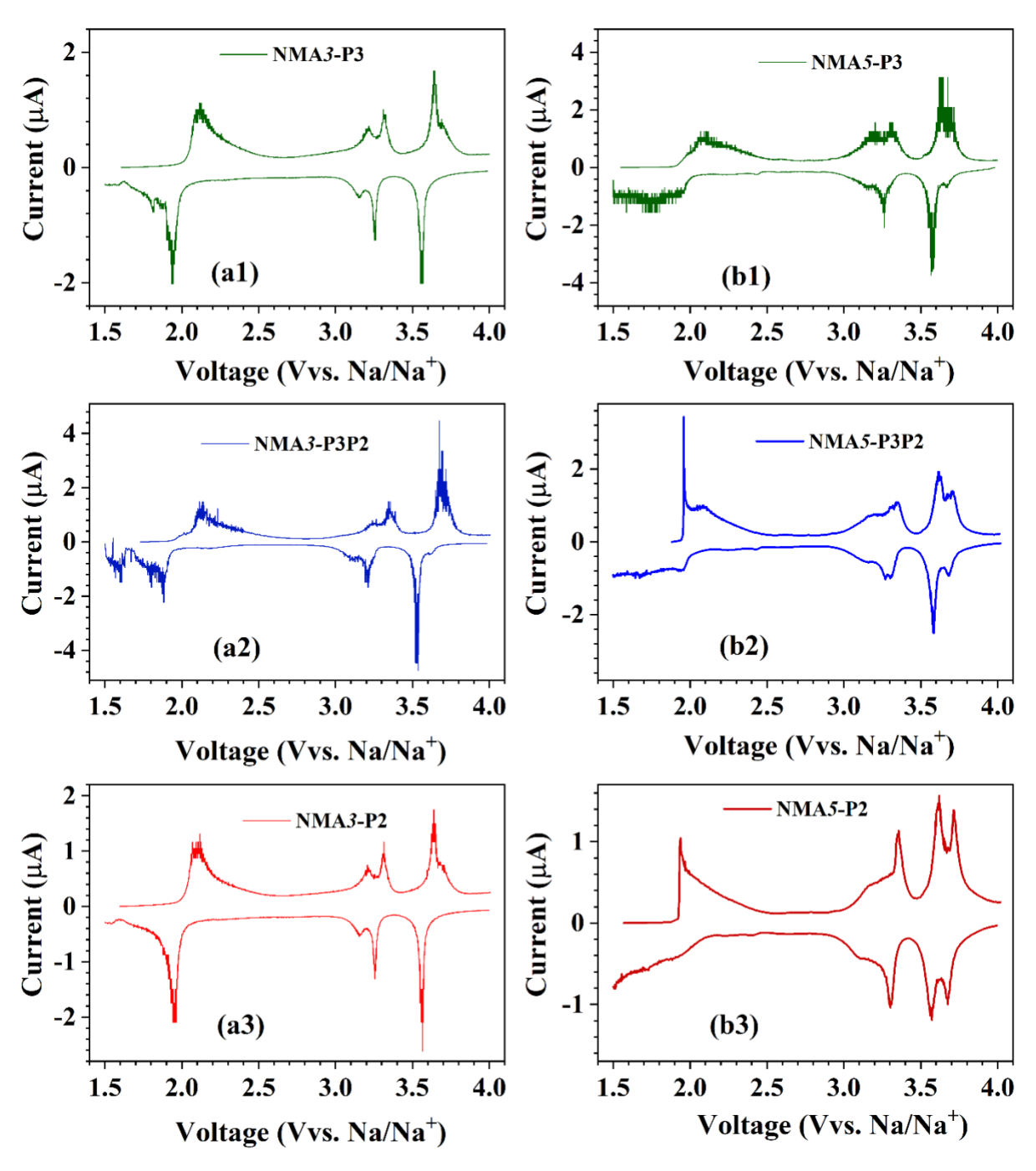


Fig. S9. dQ/dV vs. V plots of NMA3 (a1-a3) and NMA5 (b1-b3) series of cathodes cycled at 0.1C.

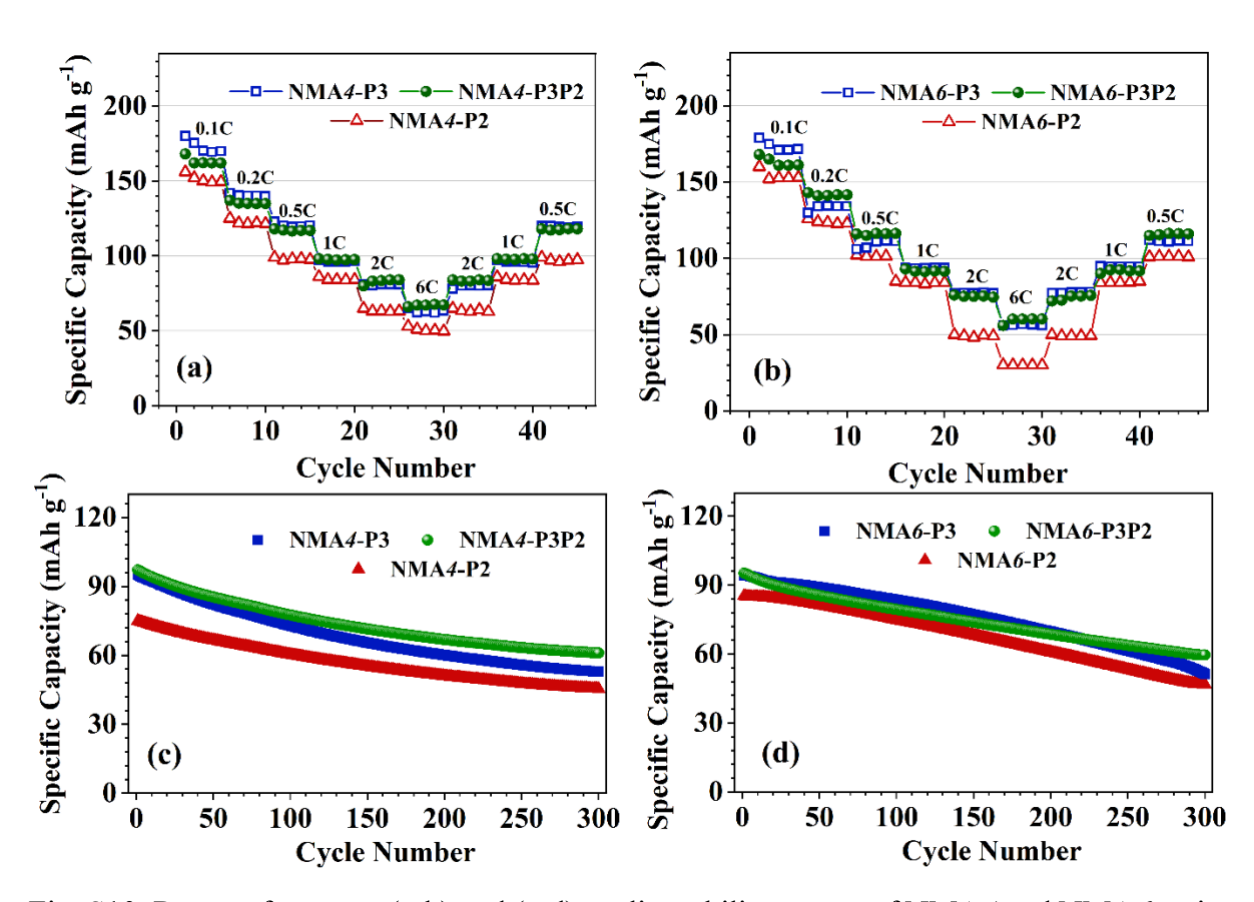


Fig. S10. Rate performance (a-b) and (c-d) cyclic stability curves of NMA4 and NMA6 series of cathodes cycled between 1.5 V - 4.0 V.

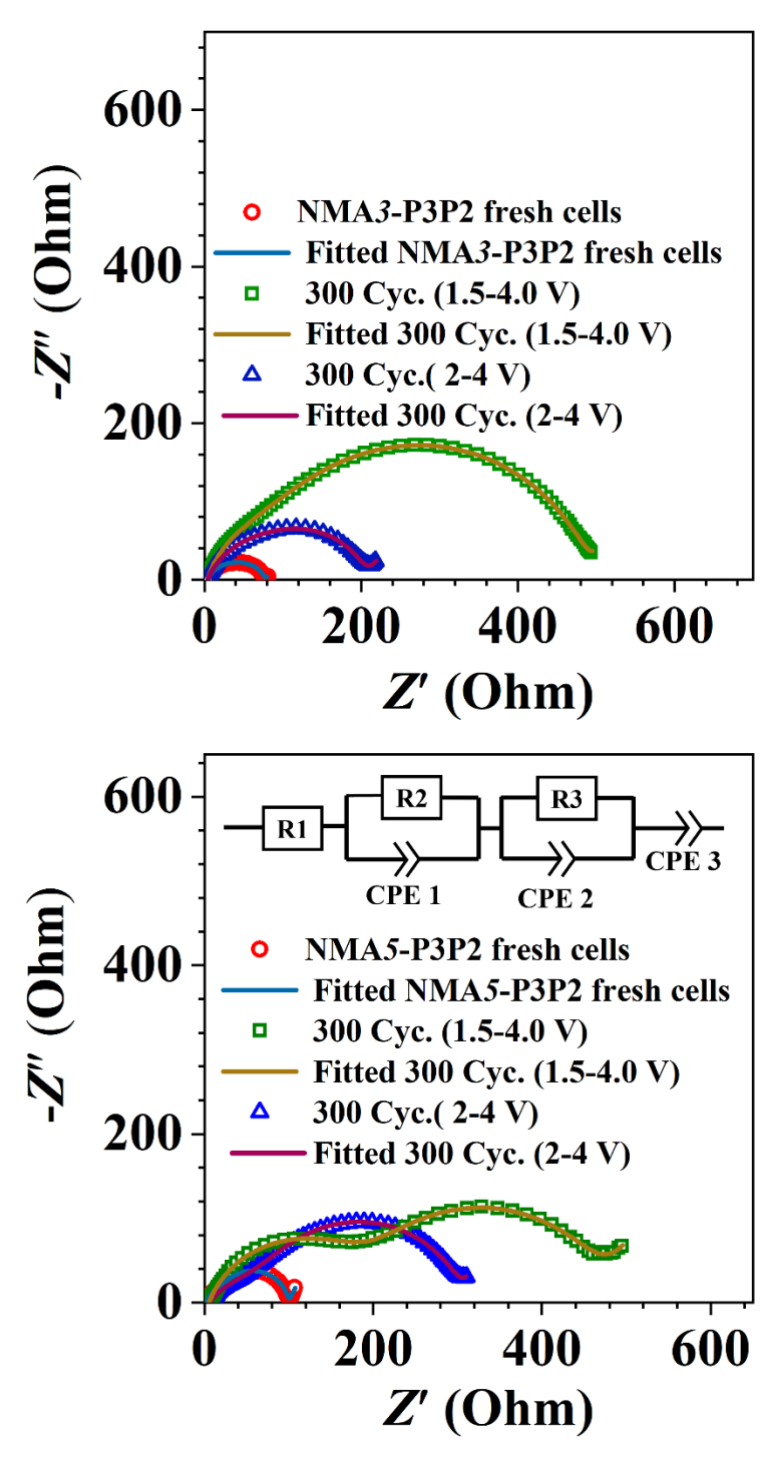


Fig. S11. Nyquist plots of NMA3-P3P2 and NMA5-P3P2 cathodes before and after cycling. Figure inset shows the equivalent circuit used to fit the impedance data.

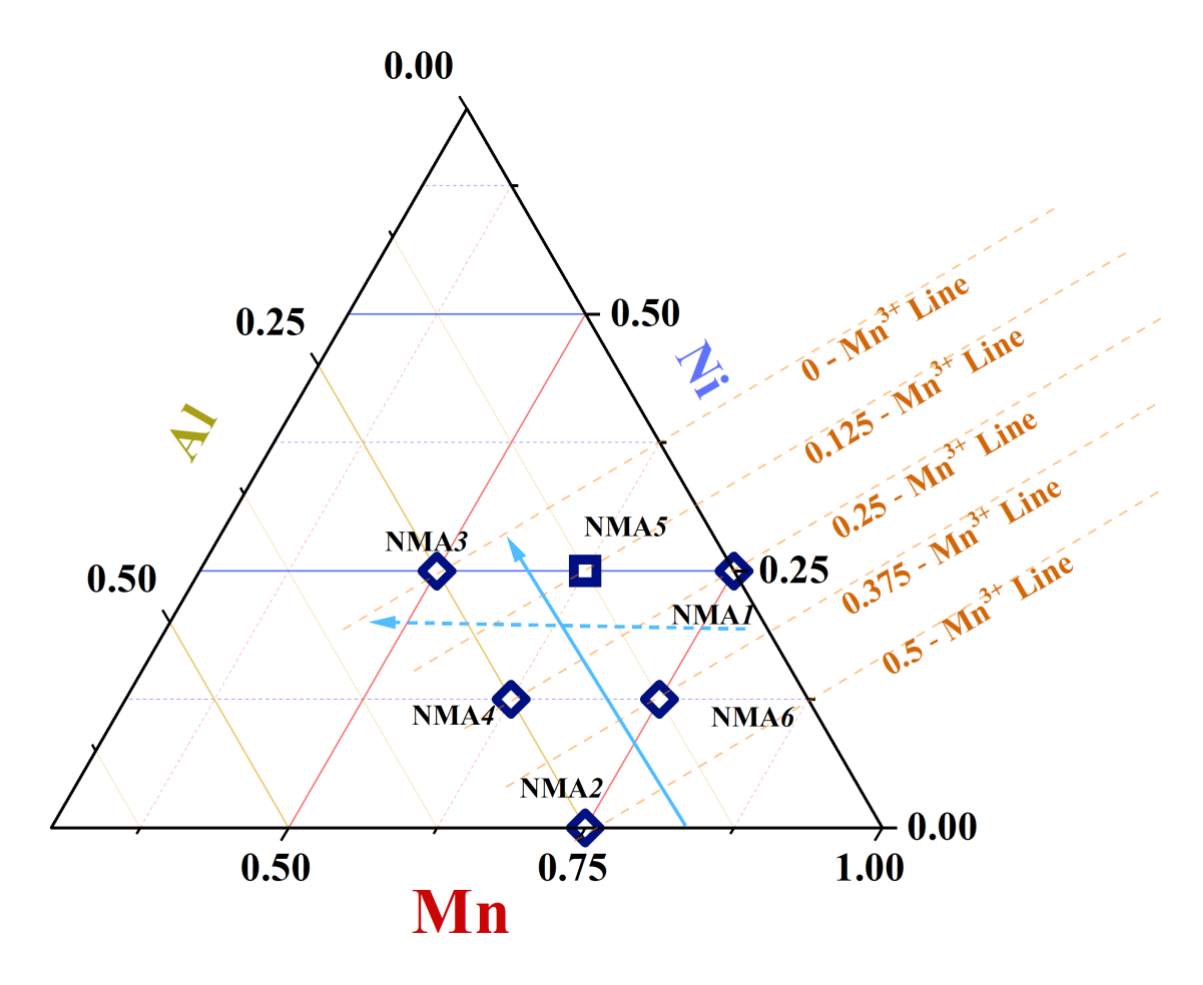


Fig. S12. Pseudo-ternary diagram of Na<sub>3/4</sub>(Mn-Al-Ni)O<sub>2</sub> system showing constant Mn<sup>3+</sup> concentration lines. The solid blue arrow indicates the increasing specific capacity, cyclability, and rate performance in compositions with constant Al<sup>3+</sup> content. The dotted arrow depicts the compositions (constant Ni<sup>2+</sup> content) along which rate performance improves.

**Table S1.** The chemical compositions of the as-prepared samples were measured by inductively coupled plasma atomic emission spectroscopy (ICP-AES).

Commis	Nominal composition	Calculated composition		
Sample -	Na/ Mn/ Ni/ Al	Na/ Mn/ Ni/ Al		
NMA3-P2	0.75/0.50/0.25/0.25	0.735/0.501 /0.252/0.247		
NMA4-P2	0.75/0.625/0.125/0.25	0.744/0.628/0.123/0.245		
NMA5-P2	0.75/0.625/0.25/0.125	0.742/0.621/0.247/0.127		
NMA6-P2	0.75/0.75/0.125/0.125	0.745/0.739/0.128/0.123		

**Table S2.** Lattice parameters of NMA3 samples obtained from the Rietveld refinement of room temperature XRD data.

Sample	Phase (Fraction)	a (Å)	c (Å)	$V(\mathring{\mathbf{A}}^3)$	Reliability Factors
NMA3-P3	P3 (100%)	2.8838 (1)	16.7924 (2)	120.97 (1)	R <sub>exp</sub> : 2.23 R <sub>wp</sub> : 2.51 R <sub>p</sub> : 1.99 GOF: 1.12
NMA3-P3P2	P3 (47.3%)	2.8864 (1)	16.773 (1)	121.00 (2)	Rexp: 2.29 Rwp: 3.41
	P2 (52.7%)	2.8842 (2)	11.164 (1)	80.42 (1)	<i>R<sub>p</sub></i> : 2.59 <i>GOF</i> : 1.48
NMA <i>3</i> -P2	P2(100%)	2.8834 (2)	11.1669 (4)	80.404 (5)	R <sub>exp</sub> : 1.98 R <sub>wp</sub> : 3.41 R <sub>p</sub> : 2.49 GOF: 1.71

**Table S3.** Lattice parameters of NMA4 samples obtained from the Rietveld refinement of room temperature XRD data.

Sample	Phase (Fraction)	a (Å)	c (Å)	V (Å <sup>3</sup> )	Reliability Factors
NMA4-P3	P3 (100%)	2.8762 (2)	16.7789 (4)	119.87 (2)	R <sub>exp</sub> : 2.49 R <sub>wp</sub> : 3.08 R <sub>p</sub> : 2.39 GOF: 1.23
NMA4-P3P2 -	P3 (50%)	2.8876 (2)	16.761 (2)	120.05 (2)	Rexp: 2.11 Rwp: 2.75
	P2 (50%)	2.8820 (1)	11.133 (2)	80.18 (1)	<i>R<sub>p</sub></i> : 2.12 GOF: 1.30
NMA <i>4</i> -P2	P2(100%)	2.8751 (3)	11.176 (2)	80.01 (1)	Rexp: 2.29 Rwp: 2.75 Rp: 2.14 GOF: 1.19

**Table S4.** Lattice parameters of NMA5 samples obtained from the Rietveld refinement of room temperature XRD data.

Sample	Phase (Fraction)	a (Å)	c (Å)	V (Å <sup>3</sup> )	Reliability Factors
NMA5-P3	P3 (100%)	2.8862 (1)	16.775 (2)	120.02 (1)	Rexp: 2.11 Rwp: 2.57
	. ,				R <sub>p</sub> : 1.98 GOF: 1.21
NMA5-P3P2	P3 (53.25%)	2.8875 (2)	16.778 (2)	120.50 (2)	Rexp: 2.09 Rwp: 2.68
	P2 (46.75%)	2.8840 (3)	11.147 (1)	80.29 (1)	R <sub>p</sub> : 1.91 GOF: 1.28
NMA5-P2	P2(100%)	2.8800 (1)	11.165 (1)	80.25 (1)	Rexp: 2.67 Rwp: 3.38 Rp: 2.66 GOF: 1.26

**Table S5.** Lattice parameters of NMA6 samples obtained from the Rietveld refinement of room temperature XRD data.

Sample	Phase (Fraction)	a (Å)	c (Å)	V (Å <sup>3</sup> )	Reliability Factors
NMA6-P3	P3 (100%)	2.8848 (1)	16.7749 (1)	120.89 (1)	Rexp: 2.01 Rwp: 2.45 Rp:1.92 GOF: 1.21
NMA6-P3P2 —	P3 (48.5%)	2.8751 (1)	16.775 (1)	120.23 (1)	Rexp: 1.90 Rwp: 2.21
	P2 (51.5%)	2.8746 (1)	11.160 (5)	79.80 (1)	<i>R<sub>p</sub></i> : 1.16 <i>GOF</i> : 1.79
NMA6-P2	P2(100%)	2.876 (2)	11.164 (4)	80.02 (2)	Rexp: 1.95 Rwp: 3.49 Rp: 2.49 GOF: 1.78

**Table S6.** The nominal concentration of  $Mn^{3+}$  and  $Mn^{4+}$  in the NMAx series of compounds.

Composition	Mn <sup>3+</sup> concentration	Mn <sup>4+</sup> concentration
Na <sub>0.75</sub> Mn <sub>0.50</sub> Ni <sub>0.25</sub> Al <sub>0.25</sub> O <sub>2</sub> (NMA3)	0	0.5
Na <sub>0.75</sub> Mn <sub>0.625</sub> Ni <sub>0.125</sub> Al <sub>0.25</sub> O <sub>2</sub> (NMA4)	0.25	0.375
Na <sub>0.75</sub> Mn <sub>0.625</sub> Ni <sub>0.25</sub> Al <sub>0.125</sub> O <sub>2</sub> (NMA5)	0.125	0.5
Na <sub>0.75</sub> Mn <sub>0.75</sub> Ni <sub>0.125</sub> Al <sub>0.125</sub> O <sub>2</sub> (NMA6)	0.375	0.375

**Table S7**. Comparison of specific capacity and cyclability for various cathode materials for sodium-ion batteries.

	Voltage	Capacity	Capacity retention,	
Material	Range vs.	(0.1C,	cycles, C-rate	
	Na <sup>+</sup> /Na	mAh g <sup>-1</sup> )	cycles, C-rate	
P2/O3	2.0–4.3 V	130	73.1%, 200 cycles,	
$Na_{0.736}Ni_{0.264}Mg_{0.1}Mn_{0.636}O_{2}[1]$	2.0 <del>-4</del> .5 V	130	1C	
P2/O3	2.0–4.5 V	181	89.6%, 100 cycles,	
Na <sub>0.80</sub> Li <sub>0.13</sub> Ni <sub>0.20</sub> Fe <sub>0.10</sub> Mn <sub>0.57</sub> O <sub>2</sub> [2]	2.0 <del>-4</del> .3 V	101	1C	
P2/O3	1.5–4.2 V	160	70%, 100 cycles,	
$Na_{0.67}Li_{0.15}Ni_{0.18}Mg_{0.02}Mn_{0.8}O_{2}$ [3]	1.5 <del>-4</del> .2 V	100	0.1C	
P2/O3	2.2–4.3 V	160	79.2%, 100 cycles,	
$Na_{0.76}Ni_{0.33}Mn_{0.50}Fe_{0.10}Ti_{0.07}O_{2}$ [4]	2.2 <del>-1</del> .5 v	100	1C	
P2-Na <sub>0.67</sub> Mn <sub>0.67</sub> Ni <sub>0.23</sub> Mg <sub>0.1</sub> O <sub>2</sub> [5]	1.5-4.0 V	120	95%, 50 cycles	
1 Z-1 <b>va</b> <sub>0.671</sub> <b>v</b> 111 <sub>0.671</sub> <b>v</b> 10.231 <b>v</b> 1g <sub>0.1</sub> O <sub>2</sub> [J]	1.3-4.0 V	.3-4.0 V 120	1C	
P2/O3	2.0-4.3 V	132.5	80.1%, 120 cycles,	
Li <sub>0.2</sub> Na <sub>0.8</sub> Ni <sub>0.33</sub> Mn <sub>0.67</sub> O <sub>2</sub> [6]	2.0 <del>-4</del> .5 V	132.3	1C	
P2/O3	2.2–4.4 V	126.6	80.6%, 200 cycles,	
Na <sub>0.85</sub> Ni <sub>0.34</sub> Mn <sub>0.33</sub> Ti <sub>0.33</sub> O <sub>2</sub> [7]	2.2— <del>1.1</del> v	120.0	1C	
P2/Tunnel/Z	2.0-4.3V	185	77%, 100 cycles,	
Na <sub>0.7</sub> MnO <sub>2.5</sub> [8]	2.0-4.5 V	103	0.5C	
P2/P3	1.5–4.0 V	182	70%, 300 cycles,	
Na <sub>0.75</sub> Mn <sub>0.50</sub> Ni <sub>0.25</sub> Al <sub>0.25</sub> O <sub>2</sub> ( <i>This work</i> )	1.5 <del>-4</del> .0 V	102	1C	
P2/P3			70%, 300 cycles,	
Na <sub>0.75</sub> Mn <sub>0.625</sub> Ni <sub>0.25</sub> Al <sub>0.125</sub> O <sub>2</sub> ( <i>This</i>	1.5–4.0 V	187.6	1C	
work)			10	

## **References:**

- [1] L. Zhang, C. Guan, J. Zheng, H. Li, S. Li, Y. Lai, Z. Zhang, Rational design of intergrowth P2/O3 biphasic layered structure with reversible anionic redox chemistry and structural evolution for Na-ions batteries, Science Bulletin, 68 (2023) 180-191 https://doi.org/10.1016/j.scib.2023.01.010.
- [2] J. Feng, D. Fang, Z. Yang, J. Zhong, C. Zheng, Z. Wei, J. Li, A novel P2/O3 composite cathode toward synergistic electrochemical optimization for sodium ion batteries, J. Power Sources, 553 (2023) 232292 https://doi.org/10.1016/j.jpowsour.2022.232292.
- [3] Y. Ding, S. Wang, Y. Sun, Q. Liu, Q. An, H. Guo, Layered cathode-Na<sub>0.67</sub>Li<sub>0.15</sub>Ni<sub>0.18</sub>Mg<sub>0.02</sub>Mn<sub>0.8</sub>O<sub>2</sub> with P2/O3 hybrid phase for high-performance Na-ion batteries, J. Alloys Compd., 939 (2023) 168780

  https://doi.org/10.1016/j.jallcom.2023.168780.
- [4] Z. Cheng, X.-Y. Fan, L. Yu, W. Hua, Y.-J. Guo, Y.-H. Feng, F.-D. Ji, M. Liu, Y.-X. Yin, X. Han, Y.-G. Guo, P.-F. Wang, A Rational Biphasic Tailoring Strategy Enabling High-Performance Layered Cathodes for Sodium-Ion Batteries, Angew. Chem. Int. Ed., 61 (2022) e202117728 https://doi.org/10.1002/anie.202117728.
- [5] C. Santamaría, E. Morales, C.d. Rio, B. Herradón, J.M. Amarilla, Studies on sodium-ion batteries: Searching for the proper combination of the cathode material, the electrolyte and the working voltage. The role of magnesium substitution in layered manganese-rich oxides, and pyrrolidinium ionic liquid, Electrochim. Acta, 439 (2023) 141654 <a href="https://doi.org/10.1016/j.electacta.2022.141654">https://doi.org/10.1016/j.electacta.2022.141654</a>.
- [6] J. Feng, S.-h. Luo, J. Cong, K. Li, S. Yan, Q. Wang, Y. Zhang, X. Liu, X. Lei, P.-q. Hou, Synthesis and electrochemical properties of Co-free P2/O3 biphasic Na<sub>1-x</sub>Li<sub>x</sub>Ni<sub>0.33</sub>Mn<sub>0.67</sub>O<sub>2</sub>

cathode material for sodium-ion batteries, J. Electroanal. Chem., 916 (2022) 116378 https://doi.org/10.1016/j.jelechem.2022.116378.

[7] L. Yu, Z. Cheng, K. Xu, Y.-X. Chang, Y.-H. Feng, D. Si, M. Liu, P.-F. Wang, S. Xu, Interlocking biphasic chemistry for high-voltage P2/O3 sodium layered oxide cathode, Energy Storage Mater., 50 (2022) 730-739 <a href="https://doi.org/10.1016/j.ensm.2022.06.012">https://doi.org/10.1016/j.ensm.2022.06.012</a>.

[8] L. Xu, Q. Ran, L. Li, Q. Hu, G. Cai, X. Liu, A multiphase coupling strategy to structurally stable manganese-based oxides cathode for high electrochemical performance sodium ion batteries, Electrochim. Acta, 467 (2023) 143085 <a href="https://doi.org/10.1016/j.electacta.2023.143085">https://doi.org/10.1016/j.electacta.2023.143085</a>.